UNIVERSITÄT
BERN

OESCHGER CENTRE
CLIMATE CHANGE RESEARCH

Optimal Operation and Analysis of the "Energiezentrale Forsthaus": A Unit Commitment Approach using Mixed Integer Linear Programming

Master Thesis

Faculty of Science, University of Bern

Student: Annika Schmidt

Supervisor: Prof. Dr. Doina Radulescu
Advisor: Miriam Moeri

Date: 25th August 2023

Abstract

The energy sector saw a significant increase in CO_2 emissions in 2022, with a substantial portion coming from heating and cooling demand due to extreme weather. To achieve decarbonization targets, the energy sector needs to prioritize improving its efficiency and integrating renewable energy. Combined heat and power (CHP) plants are highly efficient, and offer a less carbon-intensive way to generate energy from fossil fuels. This work focuses on optimizing the Energiezentrale Forsthaus (EZF), a CHP-based power plant in Bern, Switzerland. A unit commitment (UC) approach is chosen to set up a model that aims to determine the optimal mix of heat and power production which can maximize profits while satisfying heating demand. The model is solved using Mixed Integer Linear Programming (MILP). The MILP-UC model incorporates the feasible operation region (FOR) to capture the nonlinear efficiencies of CHP units. The results highlight the economic and ecological trade-offs in running CHP plants, revealing a rise in profitability due to enhanced responsiveness to price fluctuations, alongside a notable decrease in CO_2 emissions. These findings support decision-making for sustainable energy generation systems in the future, especially for the EZF.

Acknowledgement

Foremost, I would like to express my gratitude to my advisor **Miriam Moeri** for helping me find this master thesis and giving me the opportunity to work on a specific project with **ewb (Energie Wasser Bern)**. Next, I would like to express my gratitude to **Prof. Dr. Doina Radulescu** for supervising my thesis. Further, my sincere appreciation and thanks go to **Anton Luethi** for supporting me in the design and implementation of the MILP-UC model in TS-Energy. **BKW (Berner Kraftwerke)** gave me the opportunity to access a license to TS-Energy. TS-Energy is an integrated platform for the optimization of energy portfolios, developed by **Time-Steps AG** and today acquired by PSI Energy Markets GmbH. Moroever, BKW gave me the opportunity to use FICO optimizer to run and solve my MILP-UC model. Further, I want to thank **Thomas Buecherer** and **Thomas Andres** of ewb for sharing their knowledge about the power plant characteristics of the "Energiezentrale Forsthaus". Thanks to their help, I was able to define the technical constraints of the model and build up technical knowledge in the field of thermodynamics. Another thanks goes to various members of the ewb staff, especially **Fabio Fuerst**, **Marc Maurer** and **Christoph Hodel**, for interesting discussions and their valuable inputs to various topics.

Contents

Nomenclature

Abbrevations

EZF: Energiezentrale Forsthaus
CHP: combined heat and power plant
UC: unit commitment
$MILP$: mixed integer linear programming
FOR: feasible operation region
$CCGT$: combined-cycle gas turbine (GT)
$HRSG$: heat recovery steam generation
$ECST$: extraction condensing steam turbine
$BPST$: back pressure steam turbine
CSS: clean spark spread

Indices

t, hourly periods running from 1 to N_T hours
i, index for combined heat and power units running from 1 to N_{CHP}
j, index for heat-only units running from 1 to N_B
k, index for combined heat and power and heat-only units $k \in i, j$
bp, section index of power generation efficiency for CHP unit i, from 1 to N_{BP}
bh, section index of heat generation efficiency for CHP unit i, from 1 to N_{BH}

Functions

$C_{i,t}^{CHP}$: cost function of unit i at time t
$C_{j,t}^{B}$: cost function of unit j at time t

Constants

UT_k: minimum up-time of unit k [h]
DT_k: minimum down-time of unit k [h]
c_k^{SU}: start-up costs of unit k [CHF]
c_k^{SD}: shut-down costs of unit k [CHF]
H_t^D: heat demand at time t [MWth]
T_t: ambient air temperature [°C]
λ_t^H: heat price at time t [CHF/MWh]
λ_t^P: power spot price at time t [EUR/MWh]
λ_t^G: gas spot price at time t [EUR/MWh]
$\lambda_t^{CO_2,certificate}$: price for CO_2 certificate at time t [EUR/t CO_2]
$\lambda_t^{CO_2,tax}$: CO_2 incentive tax at time t [CHF/ t CO_2]
λ_t^{waste}: waste price at time t [CHF/t]
λ_t^{wood}: wood price at time t [CHF/MWh]
ROE_t: exchange rate at time t [EUR/CHF]
R_k^{up}: maximum ramp-up rate of unit k [MW/h]
R_k^{down}: maximum ramp-down rate of unit k [MW/h]

$H_j^{B,min}/H_j^{B,max}$: minimum/maximum generation limit of heat-only unit j [MWth]
η_j^B: heat generation efficiency of unit j [%]

Variables

$P_{i,t}^{CHP}$: produced power from CHP unit i at time t [MWel]
$H_{i,t}^{CHP}$: produced heat from CHP unit i at time t [MWth]
$H_{j,t}^{CHP}$: produced heat from heat-only unit j at time t [MWth]
H_t: total produced heat at time t [MWth], where $H_t = \sum_{i=1}^{N_{CHP}} H_{i,t}^{CHP} + \sum_{j=1}^{N_B} H_{j,t}^{B}$
P_t: total produced power at time t [MWel], where $P_t = \sum_{i=1}^{N_{CHP}} P_{i,t}^{CHP}$

$V_{k,t}$: binary variable for commitment status of unit k at time t
$v_{i,bp,t}^{CHP,P,eff}$: binary variable for selecting the efficiency segment of power generation of CHP unit i at time t
$v_{i,bh,t}^{CHP,H,eff}$: binary variable for selecting the efficiency segment of heat generation of CHP unit i at time t
$SU_{k,t}$: binary variable representing start-up status of unit k at time t
$SD_{k,t}$: binary variable representing shut-down status of unit k at time t

$\varphi_{i,bp,t}^{CHP,P}$: variable for linearizing constraints of selecting efficiency segment of power generation of CHP unit i at time t
$\varphi_{i,bh,t}^{CHP,H}$: variable for linearizing constraints of selecting efficiency segment of heat generation of CHP unit i at time t
$\eta_{i,bp}^{CHP,P}$: power generation efficiency of section, bp, of CHP unit i [%]
$\eta_{i,bh}^{CHP,H}$: heat generation efficiency of section, bh, of CHP unit i [%]
$\eta_{i,t}^{CHP}$: overall generation efficiency of CHP unit i at time t [%]

$X_{k,t}^{on}$: time duration for which unit k is on at time t [h]
$X_{k,t}^{off}$: time duration for which unit k is off at time t [h]
$F_{j,t}^{B}$: fuel usage of the heat-only unit j at time t [MWh]
$F_{i,t}^{CHP,P}$: fuel usage of the power output of CHP unit i at time t [MWh]
$F_{i,t}^{CHP,H}$: fuel usage of the heat output of CHP unit i at time t [MWh]
$F_{i,t}^{CHP}$: total fuel usage of power and heat output of CHP unit i at time t [MWh], where $F_{i,t}^{CHP} = F_{i,t}^{CHP,P} + F_{i,t}^{CHP,H}$
$c_{i,t}^{FOM}$: fixed operation and maintenance cost of CHP unit i at time t [CHF]
$c_{j,t}^{FOM}$: fixed operation and maintenance cost of heat-only unit j at time t [CHF]
$c_{i,t}^{VOM}$: variable operation and maintenance cost of CHP unit i at time t [CHF]
$c_{j,t}^{VOM}$: variable operation and maintenance cost of heat-only unit j at time t [CHF]
$c_{i,t}^{F}$: fuel cost of CHP unit i at time t [CHF]
$c_{j,t}^{F}$: fuel cost of heat-only unit j at time t [CHF]

Conversions

Ho = trade relevant, factor related to gross calorific value (GCV)
Hu = optimization relevant, factor related to net calorific value (NCV)

1. Introduction

Despite promising growth in renewables, in 2022 the energy sector saw the largest sectoral rise in anthropogenic CO_2 emissions. Of the total 321 Mt emissions increase, more than a fifth can be attributed to heating and cooling demand due to extreme weather (IEA, 2023). In Europe, total demand for heating and cooling accounts for almost half the energy use. Unsurprisingly, reforming the energy sector, especially, heating and cooling, is a priority to achieve decarbonization targets. We consume heating and cooling energy in three parts (residential, tertiary and industry), where household buildings represent the highest share in Europe. Traditionally, the heating and cooling sector has low efficiencies, lacks flexibility and wastes a lot of heat. However, coupling heating with the power sector allows to achieve higher efficiencies (Jimenez Navarro et al., 2018).

Among different technologies that enable us to link generating heat to generating electricity, combined heat and power (CHP) plants are of great importance thanks to their high efficiency. CHPs are the most efficient way to generate fossil-fuel based energy, and also the least carbon-intensive way to do it. CHPs can use a range of low carbon and renewable fuels including natural gas, biomethane, hydrogen or biogas (Jimenez Navarro et al., 2018). Compared to generating heat and power in separate power plants, CHPs save money and boost efficiency between 10% to 40% (Madlener & Schmid, 2003). Moreover, CHPs offer great operational and technical flexibility. Hence, they can respond fast to changes in demand and supply (J. Wang et al., 2019). CHPs are thus widely used in paper mills, agrochemical production plants, automobile factories, and rubber and steel mills (Mitra et al., 2013). Recently, CHPs have been deployed alongside other energy generation or storage technologies as part of a microgrid. So-called "smart-grids" are designed to dynamically react to time-sensitive electricity prices in case of under-utilization. For instance, CHPs act as part of virtual power plants that aim to integrate renewable energy resources such as wind or photovoltaic power (Elfarra & Kaya, 2018). By doing so, CHPs allow us to reduce the renewable curtailment via thermal energy storage. In one solution, off-peak electricity heats water in thermal storage tanks to shift daily loads (Jimenez Navarro et al., 2018). Finally, by letting CHPs interact with power reserve markets, additional benefits may be realized (Lund et al., 2012).

"ewb" (Energie Wasser Bern) is the electricity, water, gas, waste recycling and heat supply company of the city of Bern. In 2012, ewb opened the "Energiezentrale Forsthaus" (EZF). The EZF combines three CHP units: namely, a waste incinerator, a wood-fired power plant with fresh and waste wood combustion, a combined-cycle gas turbine (CCGT CHP mode) and one heat boiler. To be precise, the CCGT includes a gas turbine (GT) with heat recovery steam generation (HRSG) (Energie Wasser Bern, 2012). Thus, the EZF uses chemical properties of fuel to generate energy as well as both gas and steam technologies. By doing so, the EZF achieves higher flexibility and efficiency than other

power plants. As the EZF is coupled with Bern's district heating network, it also absorbs energy sources with low enthalpy. That is to say, a CHP system like the EZF extract heat in a late stage from the steam turbine; consequently, less energy is lost (J. Wang et al., 2019).

An operation strategy (OS) of a CHP system like the EZF exploits the flexibility during a short term dispatch in markets. A price-based OS maximizes operation profits without considering the security of a system. Contrarily, a cost-based OS aims at generating a certain output at minimum costs (J. Wang et al., 2019). The EZF must meet the city's heat demand at every hour, whereas the EZF's power production is secondary and can be economically optimized. Hence, we follow a mixed cost- and price-based OS. Notably, for each CHP unit, the power and heat production are dependent on each other since the fuel is utilized for both simultaneously. Thus, the EZF offers a constrained arbitrage opportunity among heat and power (J. Wang et al., 2019). The state of the power plant is determined by spot market prices. The EZF is a so-called price taker. Namely, its operating state does not affect market prices and we consider them as exogenous in our model (Zweifel et al., 2017).

There are two recent developments that underscore the importance of following a price-based OS for the EZF's power generation. First, the growth of non-conventional energy sources such as photovoltaics or wind parks have led to significant fluctuations in day-ahead and intra-day power prices. In contrast to fossil fuels, intermittent renewables are not unlimited in time. Unsurprisingly, renewable energy sources are given preference because they produce at low marginal costs causing the so-called merit-order effect (Zweifel et al., 2017). For instance, in the event of an energy surplus caused by good weather or winds, the power generation of the EZF could be reduced or shifted in a targeted manner. Secondly, because energy markets have started to tighten since 2021, optimizing power plants has gained even more importance. Energy prices have been rising since then due to rapid economic recovery after the pandemic, maintenance work at nuclear power plants that had been delayed, special weather conditions, and reduced investment by exporting countries as well as oil and gas companies. On top of that, following Russia's invasion of Ukraine in February 2022, the price of natural gas reached record highs in Europe (IEA, 2023). As gas frequently sets the price at which electricity is sold following the merit order, power prices increased as well (Zweifel et al., 2017). Based on these two arguments, it is crucial to determine the EZF's optimal heat and power production. This ensures optimal capacity utilization and enables responsiveness to short-term power price changes. Additionally, we hypothesize that a well-optimized EZF is also environmentally friendly in terms of CO_2 emissions. This hypothesis stems from the disparity between the affordable (even negative) prices of renewable energy sources like waste and wood, in stark contrast to those of natural gas.

Most authors address the optimal short-term scheduling of a CHP system using unit commitment (UC) (Anand et al., 2018; Arroyo & Conejo, 2004; Carrion & Arroyo,

2006; Morales-España et al., 2013; Nicolosi et al., 2021). UC is an optimization problem used to determine the short-term operation schedule of a generating unit at every hour interval under different technical and economic constraints. Thus, UC helps us to supply power and heat with the least possible losses in energy and minimum fuel consumption (Saravanan et al., 2013). However, the generation schedule must satisfy various technical constraints at every point in time; namely, the minimum up/down-time, maximum ramp up/down rate, capacity limits, unit availability and unit fuel characteristic.
Specifically, the so-called feasible operation region (FOR) defines the technical operation boundaries of a CHP unit. Makkonen and Lahdelma (2006) are the first to model the dual dependency between power and heat by a convex region. To be precise, a linear combination of the power and heat output of the extreme operation points, and linear functions of the boundary lines are used to represent the FOR. This method was further applied by Ko and Kim (2019), C. Wang et al. (2022) and Zhang et al. (2020). Depicting a FOR enables the model to implicitly account for nonlinear efficiencies and thus, more precisely estimate the operation costs. At the same time, these constraints reduce the model's freedom to choose the optimal output (Morales-España et al., 2013).

The UC problem requires solution accuracy and convergence. However, the problem size and the discrete nature of the problem constrains how useful solutions are. Up to now, the major optimization techniques for solving UC problems have included linear and nonlinear programming, dynamic programming, lagrangean relaxation, genetic algorithm, particle swarm optimization, mixed integer linear (MILP) and nonlinear programming, rolling horizon and stochastic or robust optimization. Thanks to progress in computational and algorithmic power MILP nowadays provides advantages over the other approaches (Kim & Edgar, 2014; Mitra et al., 2013; Morales-España et al., 2013; J. Wang et al., 2019). Firstly, a MILP problem provides a solution that is a global optimum. Secondly, Chang et al. (2004) point out that non-linear constraints can be easily linearized, which enhances modelling capabilities. In addition, the problem solved can be large. Finally, the technical constraints provide information for bidding strategies in the power market (Morales-España et al., 2013). For instance, Ommen et al. (2014) finds that compared to Linear Programming, Mixed Integer Programming can increase the CHP's operation hours by 17% and 25%, respectively. However, the computation time increased by 143% and 219030%.

One of the first MILP approaches for the short-term scheduling of CHP plants can be found in Seeger and Verstege (Seeger & Verstege, 1991). Arroyo and Conejo (2004) provide a common MILP formulation for the UC. Carrion and Arroyo (2006) improved the formulation by reducing the numbers of binary variables, and thus, computational burden. Aghaei and Alizadeh (2013) set up a MILP-based multi-objective problem of a CHP. Their model aimed at minimizing total operation costs and carbon emissions at the same time. More recently, Morales-España et al. (2013) presents a tighter and more compact MILP formulation of start-up and shut-down ramping in UC, which reduces

computation time even further. Simulation results showed that representing the ramps accordingly also decreases operational costs.
It is important to mention that the UC literature usually considers units at a plant level. Hence, the interactions of components within the plant are not modeled (Mitra et al., 2013). To overcome this issue, Liu et al. (2009) introduced a MILP model, which considers each power plant unit of a combined cycle combustion turbine (CCCT). They show that their model is superior to an aggregated mode model. Similarly, Mitra et al. (2013) developed a deterministic MILP model for a CHP under time-sensitive electricity prices. For that, they modelled transitional behaviors with different operating modes.

To conclude, the solution of the EZF's short-term scheduling problem strongly depends on how accurately we want to describe the physical range of operation. For instance, we could describe each power plant component by thermodynamic balance equations. However, this would require modelling non-linearities and thus, go beyond the scope of this work. Given that we consider a deterministic model and the earlier mentioned advantages of MILP, we have chosen Mixed Integer Linear Programming (MILP) to solve our problem. However, if we would consider and update uncertainty such as heat demand, spot prices and temperatures in our model, rolling horizon, stochastic or robust optimization would be necessary (Morales et al., 2014).

In this work, we present a MILP-UC approach for solving the EZF's short-term operation plannning problem. The MILP-UC model maximizes the profit obtained from hourly heat and power revenues subtracted by total operating, start-up, and shut-down costs. The results of the MILP-UC model outline the optimal mix of heat and power production for each CHP or heat-only unit, that satisfy heat demand at an hourly resolution. Whilst most papers assume fixed generation efficiencies and cost functions; the present work employs feasible operation regions (FOR) with respective generation efficiencies.
We formulate the MILP-UC model in "TS-Energy", and call FICO optimizer on to solve the problem. TS-Energy is an integrated platform for optimizing energy portfolios, and it was developed by the Paul Scherrer Institut (Time-steps AG, 2023). FICO Xpress is an optimization solver for linear programming and mixed integer linear programming (MILP). In general, MILP problems are solved using a linear-programming based branch-and-bound algorithm. During the solution process, an interior point method-based helps us finding a solution for the initial relaxed linear programming (LP) problem, followed by the branch-and-cut algorithm to improve the solution. The search process only stops when a linear integer solution is found (Chang et al., 2004; FICO, 2023).

We verify how effective our MILP-UC model is by comparing the proposed heat and power mix with the actual data from the EZF in 2022. Moreover, our model allows us to infer if an economically optimized short-term scheduling of the EZF's energy production is also ecologically optimal at the same time. Specifically, we want to see whether the optimized amount of gas burned in the CCGT and heat boiler lead to a reduction in CO_2-output compared to the status quo. This can either support or impede reaching the

climate targets of the city of Bern. According to our hypothesis, the optimized amount of gas burned highly depends on fuel input prices, spot power prices and efficiency levels of the different plant components.
In a later stage, we account for uncertainty sources in the MILP-UC model, namely spot price for power and gas. We conduct a sensitivity analysis to check how robust our results are to spot price fluctuations. By replacing the deterministic hourly forecasts with past data from 2017-2021, we show the effect of the risk variable on the optimal solution.

In essence, the goal of this work is to model and strategically optimize the EZF in order to demonstrate the trade-off between financial gains and their impact on CO_2 emissions.

The work is organized as follows. Section 2 describes the power plant and introduces the MILP-UC model along with its objective function and constraints. Additionally, the FOR and the generation efficiency of CHPs are described. Section 3 outlines how we implemented the model in TS-Energy. Moreover, we outline our underlying assumptions. Section 4 presents the results and discusses the effectiveness of our proposed model. In section 5, we analyze the impact of the optimal heat and power output on the CO_2 balance. Further, we check the model for its profitability. Also, section 5 covers a sensitivity analysis by inserting uncertainty into the model. Finally, the main conclusions are drawn in section 6.

2. Model

In this section, we briefly describe the EZF. Next, we establish a MILP-UC model that takes into account all significant project variables and defines the mathematical relationships between them. Moreover, we define the technical and economic constraints, which reduce the degree of freedom in choosing the optimal output for power and heat.

2.a. Plant description

In total, the EZF produces 360'000 MWh power and releases 290'000 MWh of district heating per year. Figure 1 depicts schematically the EZF, consisting of the three CHP units $i = 1, 2, 3$ and one heat boiler unit $j = 1$. Figure 1 reveals that the EZF contains three different steam turbines; namely, *TG1*, *TG2* and *TG3*. However, they can be driven by different CHP units i (Energie Wasser Bern, 2012).
To begin, a steam turbine expands pressurized steam to a lower pressure level and uses the extracted mechanical energy to drive an electricity generator or satisfy shaft demand. Two types of steam turbines are present in the EZF. *TG1* and *TG2* are so-called extraction condensing steam turbines (ECST). By controlling the opening degree of valves, an ECST can change the electric power and the process steam flow independently by adjusting inlet steam flow. They have one high pressure inlet stream, which is expanded into a series of stages to intermediate pressure levels. At each intermediate pressure level, steam can be removed from the turbine, called extraction. At the last stage of the turbine, steam is condensed. In contrast, a backpressure steam turbine (BPST) such as *TG3* can only remove steam from the end of the turbine at a higher pressure than the condenser pressure. Consequently, a BPST operates with a constant heat-to-power ratio (Ohji & Haraguchi, 2022; J. Wang et al., 2019).

The waste incinerator (KVA) burns 110'000 tons of waste annually. The resulting steam is either directly decoupled as heat or turns the ECST *TG1*. *TG1* is connected to a power generator either to produce power or to feed the district heating network. *TG1*'s maximum electric output is 16 MW (Energie Wasser Bern, 2012).
Second, the wood-fired power plant (HHKW) burns 112'000 tons of fresh and waste wood per year. Again, steam can be directly sent to the district heating network. Otherwise, its generated steam runs via the *TG2* or *TG3*. The choice of turbine depends on the heat demand at that time. For instance, if heat demand is high, the model should prioritize *TG3*. That is because all steam, at a higher pressure than the condenser pressure, can be used back in the thermal system. This results in higher overall efficiency (Energie Wasser Bern, 2012).
Third, the combined cycle gas turbine (CCGT CHP mode) consists of a gas turbine (GT) with supplementary firing, with a total capacity of 46 MW, coupled to a heat recovery

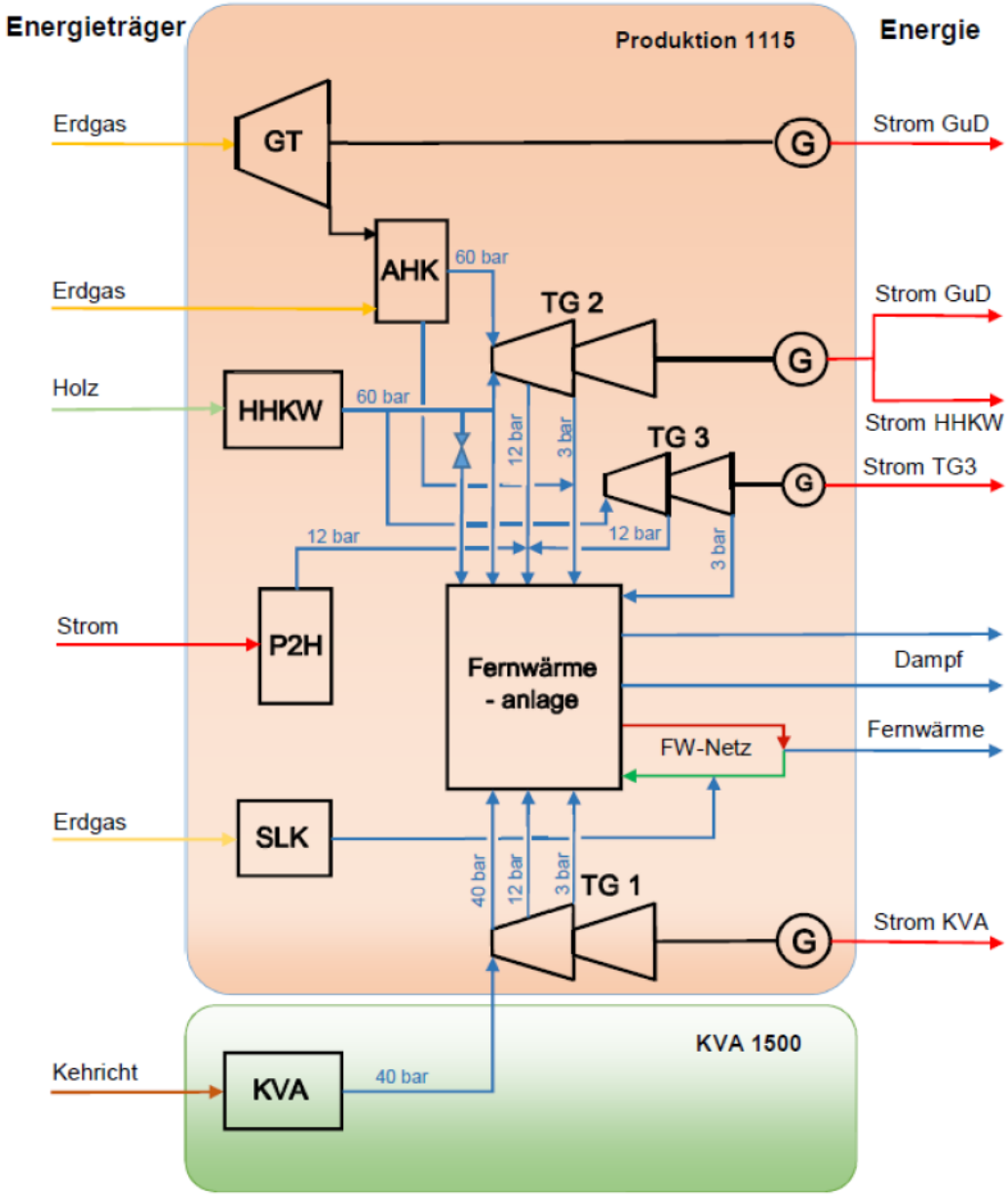

Figure 1: Schematics of the Energiezentrale Forsthaus (EZF)

steam generator (HRSG/ AHK) and the steam turbine *TG2* (Energie Wasser Bern, 2012). HRSG (AHK) are boilers that use exhaust steam from feeder GT, instead of direct combustion of gas, to generate steam in their boiler tubes. This results in higher efficiency and boosts steam production (Algie & Wong, 2002). The resulting steam from the HRSG can then produce electricity in the steam turbine *TG2* or go to the district heating network directly (Energie Wasser Bern, 2012).
Fourth, the heat boiler (SLK) is fired by gas. The boiler is designed to cover peak loads

of heat demand. Thus, it can be ramped up and down within seconds. The resulting steam is then fed into the district heating network (Energie Wasser Bern, 2012). Ultimately, the EZF contains a "power-to-heat" power plant (P2H). Yet, we do not consider P2H in our optimization problem because it is only designed for ancillary services (Energie Wasser Bern, 2012).

To conclude, the production of district heating with wood and natural gas is necessary for two reasons. First, it is needed for high heat demand in winter, which the waste incinerator alone could not cover. Second, it can be used to maximize profit and compensate for an outage of the waste incinerator, for example during an overhaul (Energie Wasser Bern, 2012).

2.b. Objective function

The objective function in our MILP-UC model maximizes total profits. The revenues result from feeding the district heating network with heat and selling electricity to the spot market. The system cost includes the units' operational cost and units' start-up and shut-down costs. We explicitly include the start-up and shut-down costs in the objective function, as we do not want the power plant to frequently turn on and off.

Precisely, the objective function is described as follows:

$$\max \sum_{t=1}^{N_T} \left((H_t \times \lambda_t^H) + (P_t \times \lambda_t^P) - \left(\sum_{i=1}^{N_{CHP}} C_{i,t}^{CHP} + \sum_{j=1}^{N_B} C_{j,t}^{B} \right) - \sum_{k \in i,j} \left(c_{k,t}^{SU} \times SU_{k,t} + c_{k,t}^{SD} \times SD_{k,t} \right) \right), \tag{1}$$

where, $i, j \in k$ represent the indices for CHP and heat-only units, respectively. H_t^D is the heat demand at time t. P_t and H_t are the total produced power and heat, and λ_t^P the forecasted power spot price at time t. The heat price λ_t^H is yearly fixed by ewb. Also, the $C_{i,t}^{CHP}$ and $C_{j,t}^{B}$ are the cost function of i^{th} CHP unit and j^{th} boiler units at time t. $c_{k,t}^{SU}$ and $c_{k,t}^{SD}$ describe the start-up/shut-down cost whereas $SU_{k,t}$ and $SD_{k,t}$ represent the binary variables of the start-up/shut-down status of the k^{th} unit at time t.

2.c. Total costs

2.c.1. Total operation costs

The general cost functions for the CHP and heat-only units are described as follows:

$$C_{i,t}^{CHP} = \sum_{i=1}^{N_{CHP}} c_{i,t}^{FOM} * V_{i,t} + (c_{i,t}^{F} + c_{i,t}^{VOM}) * F_{i,t}^{CHP}, \tag{2}$$

$$C^B_{j,t} = \sum_{j=1}^{N_B} c^{FOM}_{j,t} * V_{j,t} + (c^F_{j,t} + c^{VOM}_{j,t}) * F^B_{j,t}, \tag{3}$$

where $c^{FOM}_{k,t}$ are the fixed operation and maintenance (O&M) costs, $c^{VOM}_{k,t}$ depict the variable operation and maintenance costs and $c^F_{k,t}$ the fuel costs of unit k. The fixed O&M costs are determined by $V_{k,t}$, the binary unit commitment status of unit k $(0 = up, 1 = down)$. Similarly, the variable costs per unit k consist of fuel costs $c^F_{k,t}$ and variable O&M costs $c^{VOM}_{k,t}$. It is worth noting that the variable costs are determined by the necessary fuel consumption $F_{k,t}$ per hour t for unit k, whose derivation is later explained.

To be more precise,

$$C^{CHP}_{1,t} = (\lambda^{waste}_t * 0.295 * -1) * F^{CHP}_{1,t}, \tag{4}$$

$$C^{CHP}_{2,t} = (\lambda^{wood}_t) * F^{CHP}_{2,t}, \tag{5}$$

$$C^{CHP}_{3,t} = c^{FOM}_{3,t} * V_{3,t} + ((\lambda^G_t + (\lambda^{CO_2,C}_t * 0.202)) * ROE_t)) * (F^{CHP}_{3,t} * 1.1), \tag{6}$$

where the waste incinerator is indexed by 1, the wood-fired power plant by 2 and the CCGT by 3. For CHP unit 1, λ^{waste}_t reflects the negative waste price and 0.295 is the mean conversion factor in [t waste/MWh]. Wood price λ^{wood}_t is yearly fixed by contracts. The operating cost for the CCGT, $c^{FOM}_{3,t}$, amount to 140 CHF per hour. ROE_t describes the exchange rate in [CHF/EUR], λ^G_t represents the gas spot price and $\lambda^{CO_2,C}_t$ the price for the emissions certificate. We multiply the latter with the CO_2 emissions factor 0.202 for natural gas. Additionally, in equation (6) and equation (7) we convert the fuel consumption $F_{k,t}$ given in net calorific value (NCV) to gross calorific value (GCV) by the factor 1.1.

Respectively, the heat boiler's total costs amount to:

$$C^B_{1,t} = ((\lambda^G_t * ROE_t) + (\lambda^{CO_2,t}_t * 0.202)) * (F^B_{1,t} * 1.1), \tag{7}$$

where the heat-only unit is indexed by 1. In this case, we have to price the emissions by $\lambda^{CO_2,t}_t$, the Swiss CO_2 tax on fossil fuels. Currently, the tax amounts to CHF 120 per ton of CO_2.

2.c.2. Start-up and shut-down costs for CCGT

The start-up costs for the CCGT amounts to:

$$c^{SU}_3 = c^{FM}_3 + 2 * \lambda^P_t + (57 * 1.1 * \lambda^G_t) + c^l_3 * \lambda^H_t, \tag{8}$$

where c^{FM}_3 describe the fixed maintenance cost per start-up/shut-down process. For each cycle, 57 MW gas and 2 MW power are consumed. Further losses depend on the heat price λ^H_t and are expressed by c^l_3 equal to 10. The shut-down costs c^{SD}_3 are 0 because we included all costs in the start-up process.

2.d. Constraints

2.d.1. Energy balance constraint

The City of Bern's heat demand H_t^D must be supplied every hour t by all energy units k, as described by:

$$H_t = H_t^D, \tag{9}$$

where $H_t = \sum_{i=1}^{N_{CHP}} H_{i,t}^{CHP} + \sum_{j=1}^{N_B} H_{j,t}^{B}$. Notably, ewb is currently setting up a heat load forecast. But this goes beyond the scope of this work.

2.d.2. Commitment status constraint

In order to model the ramping behavior of the CCGT, the start-up and shut-down binary variables SU and SD are constrained as follows:

$$SU_{k,t} = V_{k,t} \times (1 - V_{k,t-1}) \quad k \in i, j, \tag{10}$$

$$SD_{k,t} = (1 - V_{k,t}) \times V_{k,t-1} \quad k \in i, j, \tag{11}$$

where $V_{k,t}$ is the binary variable for commitment status of unit k at time t.

2.d.3. Time duration for which unit k is on/off at time t

The time duration X (in hours) for which unit k is on or off at time t can be expressed as follows:

$$X_{k,t}^{on} = (X_{k,t-1}^{on} + 1) \times V_{k,t-1} \times V_{k,t} + (1 - V_{k,t-1}) \times V_{k,t} \quad k \in i, j, \tag{12}$$

$$X_{k,t}^{off} = (X_{k,t-1}^{off} + 1) \times (1 - V_{k,t-1}) \times (1 - V_{k,t}) + (V_{k,t-1}) \times (1 - V_{k,t}) \quad k \in i, j. \tag{13}$$

$X_{k,t}^{on}$ and $X_{k,t}^{off}$ are crucial for formulating the minimum up-time UT and down-time DT for unit k.

2.d.4. Minimum up/down-time constraints

We impose minimum up-time UT and down-time DT for unit k as follows:

$$(X^{on}_{k,t-1} - UT_k) \times (V_{k,t-1} - V_{k,t}) \geq 0, \quad k \in i, j, \tag{14}$$

$$(X^{off}_{k,t} - DT_k) \times (V_{k,t} - V_{k,t-1}) \geq 0, \quad k \in i, j. \tag{15}$$

Maintaining suitable UT_k and DT_k are crucial to prevent overloading power plant components within the EZF.

2.d.5. Ramp up/down constraints

We formulate the ramping-up and -down rate limits for CHP units i as follows:

$$P^{CHP}_{i,t+1} - P^{CHP}_{i,t} \leq R^{up}_i, \tag{16}$$

$$P^{CHP}_{i,t} - P^{CHP}_{i,t+1} \leq R^{down}_i, \tag{17}$$

where R^{up}_i, R^{down}_i describe the maximum ramp up/down rate of unit i, respectively. We exclude the heat boiler from equation (16) and equation (17) as it can be ramped up and down within seconds.

2.d.6. Constraints for heat-only unit

The heat boiler's fuel consumption depends on its generation efficiency η^B_j and heat output $H^B_{j,t}$ at time t:

$$F^B_{j,t} = \frac{H^B_{j,t}}{\eta^B_j} \quad \forall t, \forall j. \tag{18}$$

The heat output is limited by the capacity of the selected unit. Its minimum and maximum generation levels are given by:

$$H^{B,min}_j * V_{j,t} \leq H^B_{j,t} \leq H^{B,max}_j * V_{j,t} \quad \forall t, \forall j, \tag{19}$$

where $H^{B,min}_j$ and $H^{B,max}_j$ describe the minimum/maximum heat output for the heat boiler $j = 1$.

2.e. Feasible operation region and generation efficiency of CHP units

The heat and power outputs of the CHP units are non-separable. Thus, we depict their dependency graphically in a power-to-heat feasible operation region (FOR) by polyhedrons or linear lines (Makkonen & Lahdelma, 2006). The turbine type mentioned in section 2.a decides which representation of the FOR is accurate (Anand et al., 2018). Additionally, this section outlines the generation efficiency functions of the CHP units i.

2.e.1. FOR for a CHP using ECST

The FOR of an extraction condensing steam turbine (ECST) can be represented by a polyhedral region enclosed by the four operating points $ABCD$, as shown in figure 2. The x-axis represents the heat output in megawatts thermal and the y-axis the power output in megawatts electric. Along the boundary curve AB, the heat output increases as the power generation decreases. In contrast, the heat capacity decreases along the curve BC. According to figure 2, there are three operational factors that constrain the FOR: namely, the maximum fuel consumption AB, the minimum fuel consumption DC and the maximum heat extraction BC. We name the slopes of the boundary curves AB and BC, c_v and c_m, respectively. c_v is the influence coefficient of the heat output from the extracted steam on the electric power output when the amount of steam entering the turbine is unchanged. c_m translates to the ratio of power generation to heat output of extracted steam (Zhang et al., 2020). In other words, if the produced power of CHP unit i exceeds the maximum heat extraction boundary BC, it triggers an unwanted shut-down and restart. Also, it is not efficient to schedule a CHP unit to run at its minimum fuel consumption DC (Alipour et al., 2014; Ko & Kim, 2019).

The optimal power and heat output, $P_{i,t}^{CHP}$ and $H_{i,t}^{CHP}$, must satisfy the following four conditions if CHP unit i is committed ($V_{i,t} = 1$) at time t.

First, the operating condition within the segment of maximum fuel consumption is defined as

$$P_{i,t}^{CHP} \leq \frac{P_{i,A}^{CHP} - P_{i,B}^{CHP}}{H_{i,A}^{CHP} - H_{i,B}^{CHP}} * (H_{i,t}^{CHP} - H_{i,A}^{CHP}) + P_{i,A}^{CHP} \quad \forall t. \tag{20}$$

Second, the operating condition within the segment of maximum heat extraction is specified as

$$P_{i,t}^{CHP} \geq \frac{P_{i,B}^{CHP} - P_{i,C}^{CHP}}{H_{i,B}^{CHP} - H_{i,C}^{CHP}} * (H_{i,t}^{CHP} - H_{i,B}^{CHP}) + P_{i,B}^{CHP} \quad \forall t. \tag{21}$$

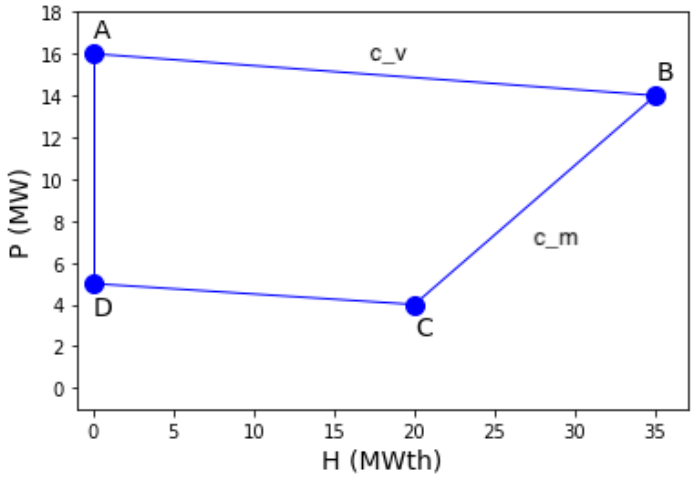

Figure 2: Power-to-heat feasible operation region for a CHP using ECST

Third, the operating condition within the segment of minimum fuel consumption translates to

$$P_{i,t}^{CHP} \geq \frac{P_{i,C}^{CHP} - P_{i,D}^{CHP}}{H_{i,C}^{CHP} - H_{i,D}^{CHP}} * (H_{i,t}^{CHP} - H_{i,C}^{CHP}) + P_{i,C}^{CHP} \quad \forall t. \tag{22}$$

Finally, the minimum and maximum operation region is constrained by

$$0 \leq P_{i,t}^{CHP} \leq P_{i,A}^{CHP} * V_{i,t} \quad \forall t, \tag{23}$$

$$0 \leq H_{i,t}^{CHP} \leq H_{i,B}^{CHP} * V_{i,t} \quad \forall t, \tag{24}$$

where $P_{i,A}^{CHP}$ and $H_{i,B}^{CHP}$ are the maximum operating points of power and heat generation.

2.e.2. FOR for a CHP using BPST

The FOR of a backpressure steam turbine (BPST) can be represented by a straight line between the extreme points E and F as shown in figure 3. This is because heat and power output are always in a constant relationship (Anand et al., 2018).

This relationship is given by:

$$P_{i,t}^{CHP} = \frac{P_{i,E}^{CHP} - P_{i,F}^{CHP}}{H_{i,E}^{CHP} - H_{i,F}^{CHP}} * (H_{i,t}^{CHP} - H_{i,E}^{CHP}) + P_{i,E}^{CHP}, \tag{25}$$

$$0 \leq H_{i,t}^{CHP} \leq H_{i,F}^{CHP} * V_{i,t} \quad \forall t, \tag{26}$$

$$0 \leq P_{i,t}^{CHP} \leq P_{i,F}^{CHP} * V_{i,t} \quad \forall t, \tag{27}$$

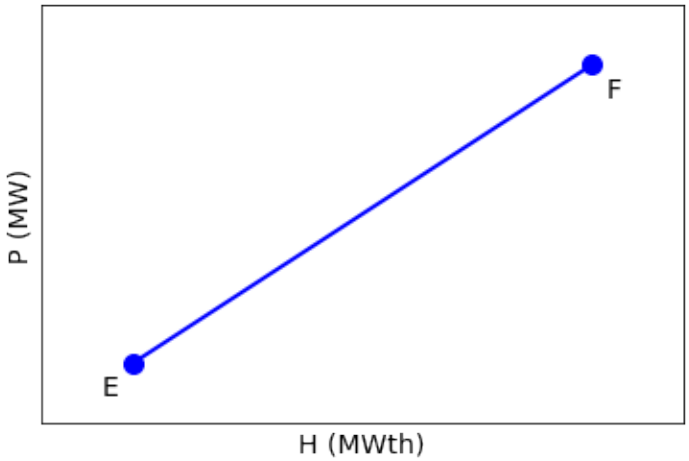

Figure 3: Power-to-heat feasible operation region for a CHP using BPST

where point E equates minimum fuel consumption, corresponding to minimum heat and power output and F stands for maximum fuel consumption with maximum heat and power output.

2.e.3. FOR for CCGT

Figure 4 demonstrates that a CCGT with HRSG can be modelled as polyhedron. However, there are three specific operating factors that limit the FOR of a CCGT, namely sustaining compressor, combustion and expansion turbine reaction, power-to-heat trade-off limits, and fuel consumption rate. In particular, it is crucial to match the intake air compression ratio and fuel consumption rate to ensure uninterrupted power generation. If the power output falls below CD (minimum fuel consumption), the fuel combustion will not produce enough gas to enable the compressor to draw in sufficient air to fully burn the fuel. As a result, the turbine power decreases, reducing the power available to the generator and compressor, leading to a phenomenon known as compressor stall (Algie & Wong, 2002). A part of power generation capacity can be traded-off for increase in energy exhaust at a fixed fuel consumption rate. In that case, more exhaust gas exits the turbine stage and the air is hotter. This allows more steam to be generated by the HRSG. Nevertheless, if the power-to-heat ratio is pushed beyond boundary curve BC (maximum heat extraction) the combustion flame can be blown out and unplanned shut down and restart occurs. Contrarily, if we operate below the boundary curve AD, illustrating minimum heat extraction (red line), back pressure flame-out can occur (Algie & Wong, 2002).

In addition, a CCGT's boundary points $ABCD$ depend on the ambient air temperature T. This means if air is denser during cooler conditions, the GT will take in more air through

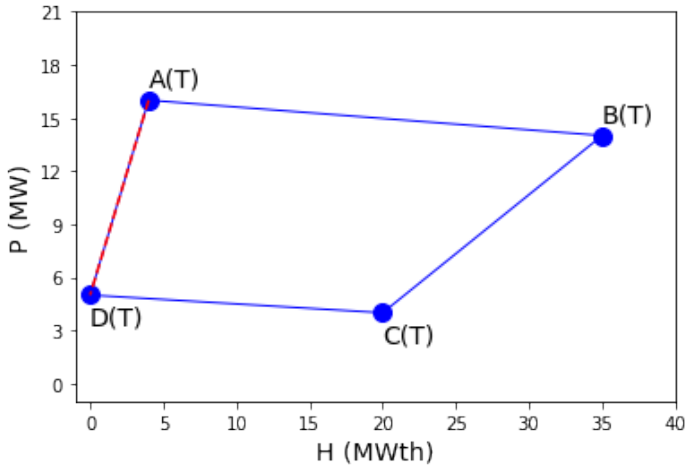

Figure 4: Power-to-heat feasible operation region for a CCGT

the compressors and turbine efficiencies improve. Hence, power generation increases. Oppositely, during hot weather, GT efficiency decreases, along with the maximum power output (Algie & Wong, 2002; González-Díaz et al., 2017). To conclude, total power output and overall efficiency of a CCGT decreases with increasing temperature.

Hence, we adapt equation (20) to equation (24) for the CCGT as follows:

$$P_{3,t}^{CHP} \leq \frac{P_{3,A}^{CHP}(T) - P_{3,B}^{CHP}(T)}{H_{3,A}^{CHP}(T) - H_{3,B}^{CHP}(T)} * (H_{3,t}^{CHP} - H_{3,A}^{CHP}(T)) + P_{3,A}^{CHP}(T), \tag{28}$$

$$P_{3,t}^{CHP} \geq \frac{P_{3,B}^{CHP}(T) - P_{3,C}^{CHP}(T)}{H_{3,B}^{CHP}(T) - H_{3,C}^{CHP}(T)} * (H_{3,t}^{CHP} - H_{3,B}^{CHP}(T)) + P_{3,B}^{CHP}(T), \tag{29}$$

$$P_{3,t}^{CHP} \geq \frac{P_{3,C}^{CHP}(T) - P_{3,D}^{CHP}(T)}{H_{3,C}^{CHP}(T) - H_{3,D}^{CHP}(T)} * (H_{3,t}^{CHP} - H_{3,C}^{CHP}(T)) + P_{3,C}^{CHP}(T), \tag{30}$$

$$P_{3,t}^{CHP} \leq \frac{P_{3,A}^{CHP}(T) - P_{3,D}^{CHP}(T)}{H_{3,A}^{CHP}(T) - H_{3,D}^{CHP}(T)} * (H_{3,t}^{CHP} - H_{3,D}^{CHP}(T)) + P_{3,D}^{CHP}(T), \tag{31}$$

$$0 \leq H_{3,t}^{CHP} \leq H_{3,B}^{CHP}(T) * V_{3,t} \quad \forall t, \quad where \quad (A \geq B), \tag{32}$$

$$0 \leq P_{3,t}^{CHP} \leq P_{3,A}^{CHP}(T) * V_{3,t} \quad \forall t, \tag{33}$$

where T represents the ambient air temperature. Unlike in section 2.e.1, we include an additional boundary constraint for minimum heat extraction with equation (31).

For simplicity, we linearize the relationship between ambient temperature T [°C] and the boundary points $ABCD$, which we denote by the indice s.

We set up the following equations for each boundary point s with respect to power and heat:

$$P_{3,s}^{CHP}(T) = \frac{P_{3,s}^{CHP}(T_{max,eff}) - P_{3,s}^{CHP}(T_{min,eff})}{T_{max,eff} - T_{min,eff}} * T_t + P_{3,s}^{CHP}(T_{max,eff}), \quad (34)$$

$$H_{3,s}^{CHP}(T) = \frac{H_{3,s}^{CHP}(T_{max,eff}) - H_{3,s}^{CHP}(T_{min,eff})}{T_{max,eff} - T_{min,eff}} * T_t + H_{3,s}^{CHP}(T_{max,eff}), \quad (35)$$

where $T_{max,eff} = -20C$ and $T_{min,eff} = 35C$.

2.e.4. Efficiency functions of CHP

The generation efficiency of a CHP is not constant, but depends on the loading level of power and heat generation over the FOR. As MILP involves integer variables that can only take on specific values, we have to model the efficiency functions of the CHP units as discrete functions (Ko & Kim, 2019). The efficiency functions illustrate the relationship between generation efficiency and power/ heat output, as shown in figure 6. The boundary points $ABCD$ cut the FOR in so-called efficiency segments with respect to heat (x-axis) and power (y-axis), as shown in figure 5. Yet, for a reasonable approximation, we model the efficiency functions by the mean value of the generation efficiency over the segments on the FOR (Ko & Kim, 2019).

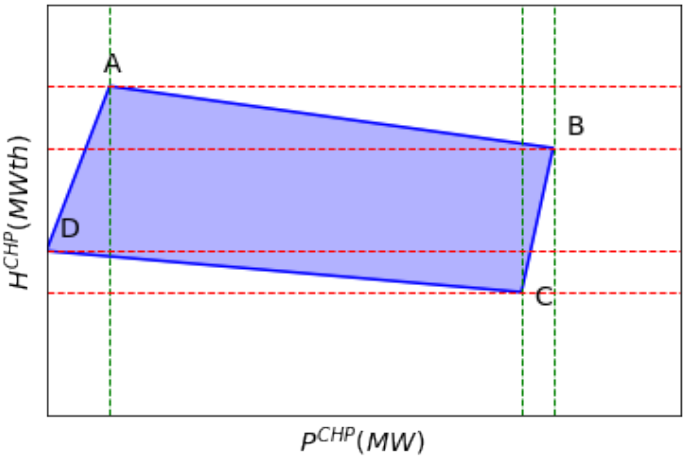

Figure 5: Efficiency segments of a feasible operation region

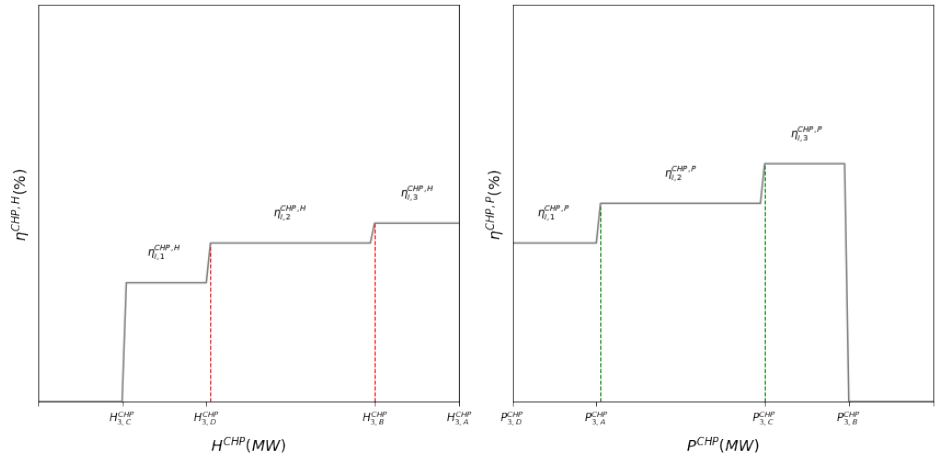

Figure 6: Heat (left) and power (right) generation efficiency functions for CHP units

Consequently, we create variables for selecting efficiency segments

$$\begin{aligned} v_{i,bp,t}^{CHP,eff,P} &\in 0,1 \quad \forall bp, \forall t, \\ v_{i,bh,t}^{CHP,eff,H} &\in 0,1 \quad \forall bh, \forall t, \end{aligned} \tag{36}$$

where bp and bh are the section indices of power and heat generation efficiency function, respectively. In other words, each of these variables is equal to 1 if the CHP unit i generates power or heat in the corresponding boundary segment and is 0 otherwise.

The generation output must be defined in the boundary segments of efficiency functions. So, we can guarantee that the generation output lies within the FOR. Thus, we bind the power and heat generation as

$$\begin{cases} P_{i,t}^{CHP} \leq (1 - v_{i,bp,t}^{CHP,eff,P}) * Z + v_{i,bp,t}^{CHP,eff,P} * P_{i,bp+1}^{CHP}, & \forall i, \forall bp, \forall t, \\ P_{i,t}^{CHP} \geq (1 - v_{i,bp,t}^{CHP,eff,P}) * Z + v_{i,bp,t}^{CHP,eff,P} * P_{i,bp}^{CHP}, & \forall i, \forall bp, \forall t, \\ H_{i,t}^{CHP} \leq (1 - v_{i,bh,t}^{CHP,eff,H}) * Z + v_{i,bh,t}^{CHP,eff,H} * H_{i,bh+1}^{CHP}, & \forall i, \forall bh, \forall t, \\ H_{i,t}^{CHP} \geq (1 - v_{i,bh,t}^{CHP,eff,H}) * Z + v_{i,bh,t}^{CHP,eff,H} * H_{i,bh}^{CHP}, & \forall i, \forall bh, \forall t, \end{cases} \tag{37}$$

where Z is an arbitrary large constant close to positive infinity.

The boundary segment can be either selected once or not at all:

$$\begin{aligned} \sum_{bp=1}^{N_{BP}} v_{i,bp,t}^{CHP,eff,P} &= V_{i,t}^{CHP} \\ \sum_{bh=1}^{N_{BH}} v_{i,bh,t}^{CHP,eff,H} &= V_{i,t}^{CHP} \end{aligned} \tag{38}$$

With equation (37) and equation (38), we can select the boundary segments according to the generation output (mix between power and heat).

Finally, the fuel consumption of CHP unit i is defined as

$$\begin{aligned} F_{i,t}^{CHP,P} &= \sum_{bp=1}^{N_{BP}} \left(\frac{P_{i,t}^{CHP}}{\eta_{i,bp}^{CHP,P}} * v_{i,bp,t}^{CHP,eff,P}\right) \quad \forall i, \forall t, \\ F_{i,t}^{CHP,H} &= \sum_{bh=1}^{N_{BH}} \left(\frac{H_{i,t}^{CHP}}{\eta_{i,bh}^{CHP,H}} * v_{i,bh,t}^{CHP,eff,H}\right) \quad \forall i, \forall t, \end{aligned} \tag{39}$$

where $P_{i,t}^{CHP}$ and $H_{i,t}^{CHP}$ describe the generation output, divided by the efficiency of the determined boundary segment $\eta_{i,bp}^{CHP,P}$ and $\eta_{i,bh}^{CHP,h}$, respectively. The latter are chosen by the above mentioned processes.

Nevertheless, the fuel consumption must be linearized for MILP optimization. This is because the constraints on fuel consumption of CHP unit i correspond to the product of variables. We detail the linearization process in appendix A.

3. Model implementation and assumptions

In this section, we explain how we implement the proposed model in section 2 in TS-Energy. Section 3.b describes our model's underlying assumptions. For the solution process, we set the MIP optimality gap equal to 0.01. The choice of the optimality gap is a trade-off between solution quality and computational time. Hence, we allow FICO solver to terminate when it reaches a solution that is within 1% of the optimal solution. For a detailed description of the MILP solution process, we refer to appendix C.

3.a. Model implementation in TS-Energy

In general, MILP problems are of the form:

Objective:	minimize $c^T x$
Constraints:	$Ax = b$ (linear constraints)
	$l \leq x \leq u$ (bound constraints)
	some or all x_j must take integer values (integrality constraints),

where linear constraints (equalities) represent exact relationship between variables. In contrast, bound constraints (inequalities) define a range of values that a variable can take. The integrality constraints allow MIP models to capture the discrete nature of some decisions. That is to say, a binary variable, whose values are restricted to 0 or 1, decides whether some action is taken or not (FICO, 2023).
TS-Energy allows us to enter the constraints described in section 2.d via linear, bound, and integrality constraints. We proceed as follows: First, we model the EZF's plant components described in section 2.a as so-called *operating units*. In the simplest form, a power plants needs three operating units, namely an input variable, a binary integer variable, which decides if the power plant is on or off, and an output variable. On each operating unit, we set so-called *payoffs* to either model the costs or revenue generated by it. We model the feasible operation region (FOR) described in section 2.e by linear equations that connect the different operating units over the corresponding binary variable. Moreover, we formulate mass balances between different operating units by balance equations (for details see appendix B). For instance, when steam is first collected from two different CHP units before it runs onto the steam turbine. Hence, TS-Energy allows us to model the EZF's physical range of operation more accurately compared to section 2. Next, as we follow an UC approach, we impose a heat supply contract to be delivered. For that, we attach heat sources from the different units k that can potentially fulfill the heat contract. Finally, FICO solver finds the optimal solution for all input and output variables that satisfy heat demand at hour t. At the same time, the solution maximizes revenue by selling surplus power to the spot market.

3.a.1. Heat boiler (SLK)

The heat boiler (heat-only unit 1) consists of three operating units, namely SLK_Gas, SLK_Heat, and the integer variable SLK_Bin, shown in figure 7.

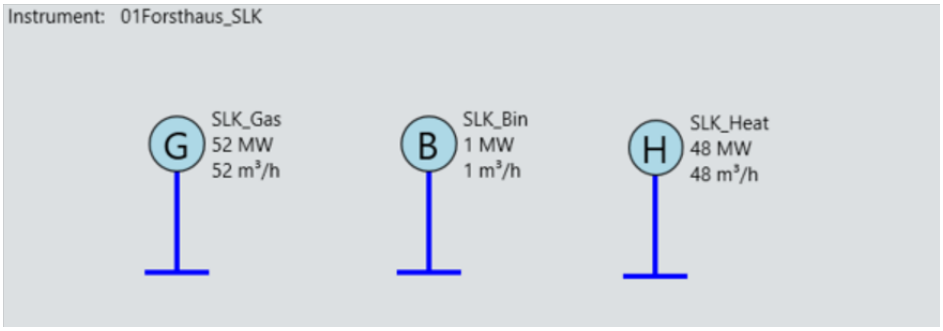

Figure 7: Operating units of heat boiler in TS-Energy

The heat boiler's minimum fuel consumption is limited by:

$$0 \leq \text{SLK\_Gas} - \text{SLK\_Gas\_min} * \text{SLK\_Bin} \leq 1000, \tag{40}$$

where 1000 represents here and in the following an arbitrarily high number in megawatts.

The heat boiler's maximum fuel consumption is bound by:

$$0 \leq \text{SLK\_Gas\_max} * \text{SLK\_Bin} - \text{SLK\_Gas} \leq 1000. \tag{41}$$

The relationship between gas and heat output is expressed as follows:

$$0 \leq \text{SLK\_Heat} + m_1 * \text{SLK\_Gas} + n_1 * \text{SLK\_Bin} \leq 0, \tag{42}$$

where the slope m_1 and the y-axis offset n_1 implicitly inherit the efficiency function described in section 2.d.6. Figure 8 shows the gas-to-heat conversion defined in equation (42) graphically.

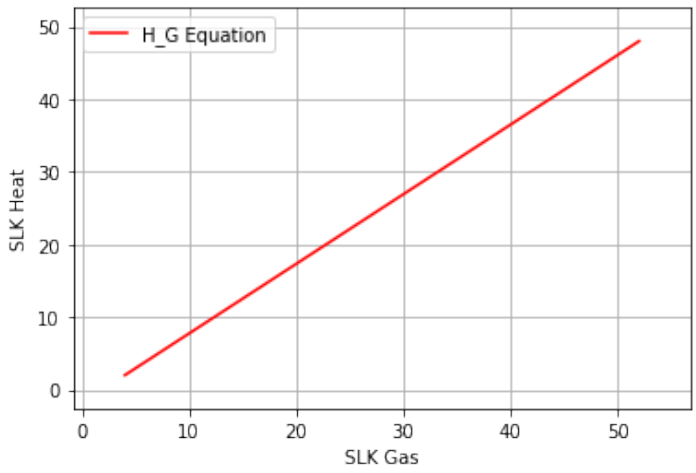

Figure 8: Gas-to-heat conversion of heat boiler in MW

3.a.2. Waste incinerator (KVA)

Figure 9 reveals that the waste incinerator is modelled via eight operating units in TS-Energy.

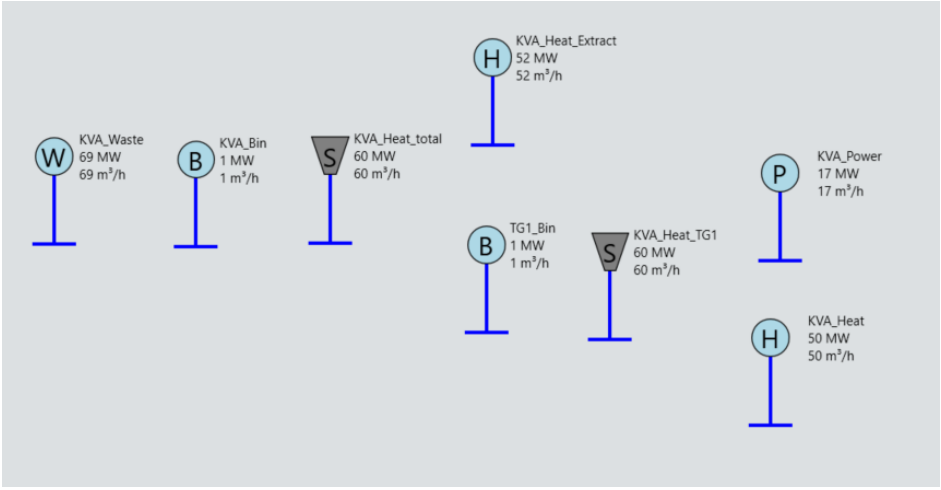

Figure 9: Operating units of waste incinerator in TS-Energy

The minimum/ maximum waste consumption are bound by:

$$0 \leq \text{KVA\_Waste} - \text{KVA\_Waste\_min} * \text{KVA\_Bin} \leq 1000, \tag{43}$$

$$0 \leq \text{KVA\_Waste\_max} * \text{KVA\_Bin} - \text{KVA\_Waste} \leq 1000. \tag{44}$$

The relationship between waste and total steam production follows:

$$0 \leq 0 - \text{KVA\_Heat\_total} + m_2 * \text{KVA\_Waste} + n_2 * \text{KVA\_Bin} \leq 0, \tag{45}$$

which is graphically depicted in figure 10. The slope m_2 describes the efficiency of how much steam can be produced per MW of waste burnt.

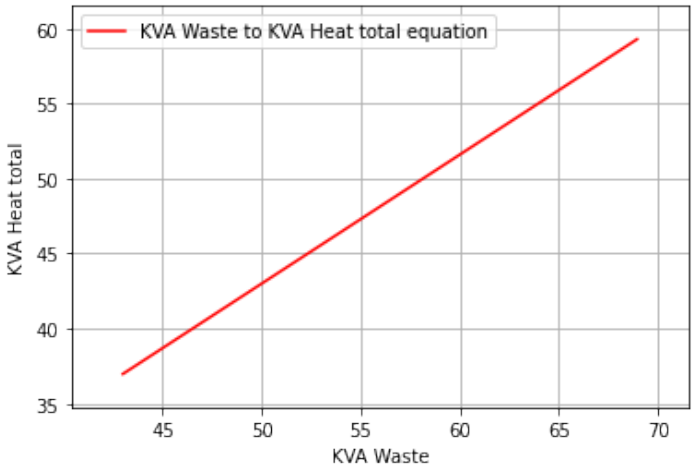

Figure 10: Waste-to-steam conversion of waste incinerator in MW

Next, the generated steam can either be directly extracted at 40 bar and sent to the district heating network or run via the ECST *TG1*. The following balance equation ensures that the sum of extracted steam (KVA_Heat_Extract) and steam passing through *TG1* (KVA_Heat_TG1) cannot exceed total steam production KVA_Heat_total.

$$0 \leq \text{KVA\_Heat\_Extract} + \text{KVA\_Heat\_TG1} - \text{KVA\_Heat\_total} \leq 0 \tag{46}$$

The minimum/ maximum steam input that can enter ECST *TG1* are bound by:

$$0 \leq \text{KVA\_Heat\_TG1} - \text{KVA\_Heat\_TG1\_min} * \text{TG1\_Bin} \leq 1000, \tag{47}$$

$$0 \leq \text{KVA\_Heat\_TG1\_max} * \text{TG1\_Bin} - \text{KVA\_Heat\_TG1} \leq 1000. \tag{48}$$

To restrict the maximum extracted steam to 52 MW, we define:

$$0 \leq \text{KVA\_Heat\_Extract} \leq 52. \tag{49}$$

Next, to model the feasible operation region (FOR) and the associated fuel consumption (KVA_Heat_TG1) of ECST *TG1* following section 2.e.1, we set up three expressions.

Note that when we discuss fuel consumption, we are referring to the steam input that enters ECST *TG1*.

First, at minimum fuel consumption, power and heat can be converted as follows:

$$-1000 \leq -\text{KVA\_Power} + o_2 * \text{KVA\_Heat} + p_2 * \text{KVA\_Bin} \leq 0. \tag{50}$$

Second, at maximum fuel consumption, power and heat can be converted as follows:

$$0 \leq -\text{KVA\_Power} + q_2 * \text{KVA\_Heat} + r_2 * \text{KVA\_Bin} \leq 1000. \tag{51}$$

Figure 11 illustrates the lower and upper bound of *TG1*. From figure 11 we can deduce how much heat can be exchanged for power at either minimum or maximum fuel consumption.

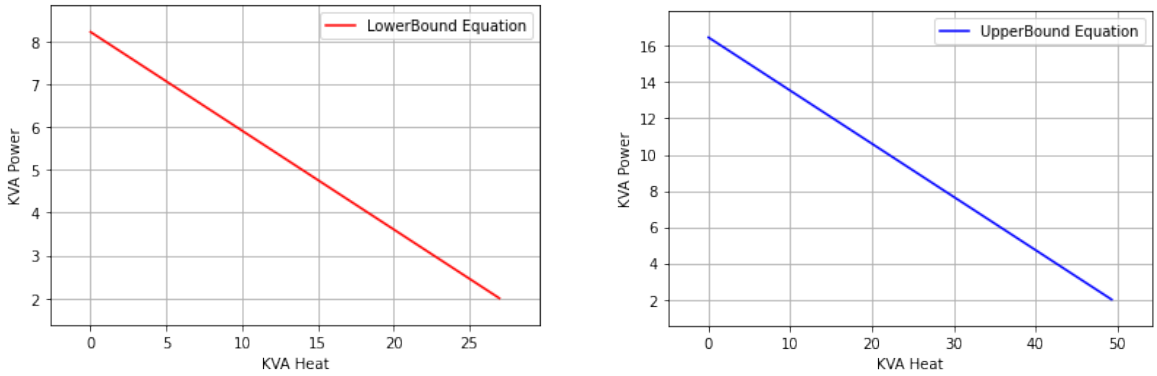

(a) Lower Bound Equation **(b)** Upper Bound Equation

Figure 11: Heat-to-power conversion via ECST *TG1* in MW

Finally, we set up a plane equation to approximate the relationship between heat and power at various fuel consumption levels. In other words, for each steam input level that satisfies equation (47) and equation (48), there exists a possible combination of power and heat.
Hence, we create a three-dimensional space with steam input (KVA_Heat_TG1) as the y-axis, power output (KVA_Power) as the x-axis and heat output (KVA_Power) as the z-axis. This space is represented in figure 12. We then plot the extreme boundary points *ABCD*, which were discussed in section 2.e.1, within this space. However, figure 12 reveals that the extreme points *ABCD* do not lie exactly on the same plane. Therefore, we define the plane equation using the method of least-squares (LS).

Hence, we set up:

$$0 \leq -a_2 * \text{KVA\_Heat\_TG1} + b_2 * \text{KVA\_Power} + c_2 * \text{KVA\_Heat} + d_2 * \text{KVA\_Bin} \leq 0. \tag{52}$$

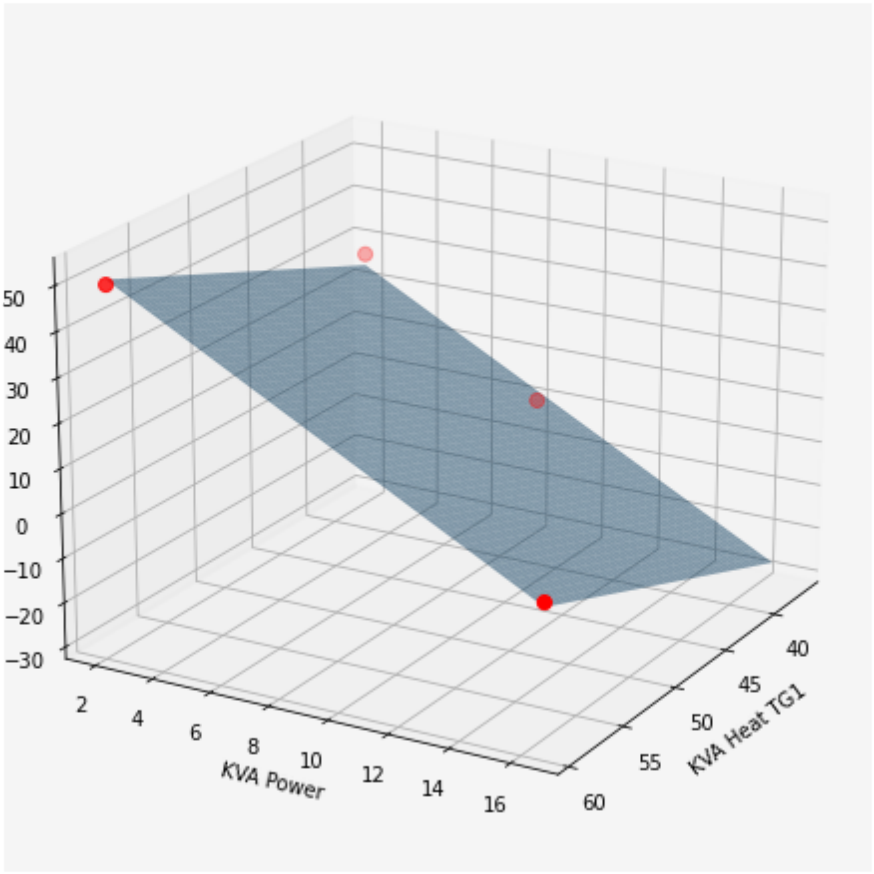

Figure 12: Plane equation of *TG1* in MW

3.a.3. CCGT (GuD) and wood-fired power plant (HHKW)

As both the CCGT and wood-fired power plant can run over the same ECST *TG2*, we combine them into a single instrument. Figure 13 illustrates the instrument, consisting of 19 operating units in TS-Energy.

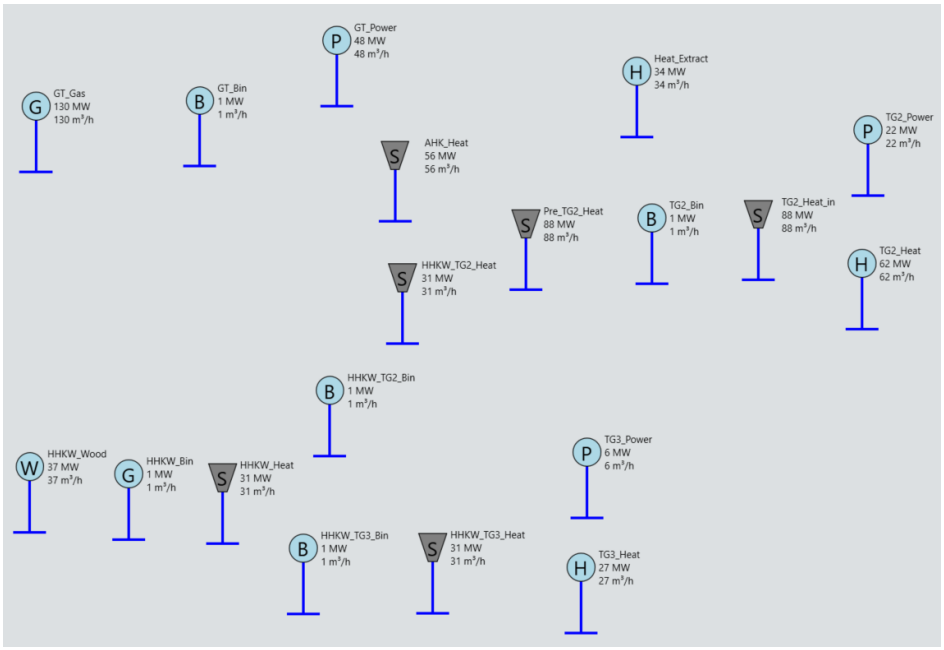

Figure 13: Operating units of CCGT and wood-fired power plant in TS-Energy

CCGT including GT with HRSG

The minimum/ maximum gas intake is governed by:

$$0 \leq \text{GT\_Gas} - \text{GT\_Gas\_min} * \text{GT\_Bin} \leq 1000, \tag{53}$$

$$0 \leq \text{GT\_Gas\_max} * \text{GT\_Bin} - \text{GT\_Gas} \leq 1000. \tag{54}$$

Here, the minimum and maximum gas consumption are influenced by the ambient air temperature (see section 2.e.3).

The relationship between gas input and the gas turbine's power generation is defined as:

$$0 \leq -\text{GT\_Power} + m_3 * \text{GT\_Gas} + n_3 * \text{GT\_Bin} \leq 0. \tag{55}$$

The coefficient m_3 captures the temperature-dependent efficiency of the gas turbine's power output.

Similarly, the relationship between gas input and the HRSG's steam generation is given by:

$$0 \leq -\text{AHK\_Heat} + o_3 * \text{GT\_Gas} + p_3 * \text{GT\_Bin} \leq 0. \tag{56}$$

Here, o_3 captures the temperature-dependent efficiency of the HRSG's steam production.

Wood-fired power plant

The minimum/ maximum wood consumption is regulated by:

$$0 \leq \text{HHKW\_Wood} - \text{HHKW\_Wood\_min} * \text{HHKW\_Bin} \leq 1000, \tag{57}$$

$$0 \leq \text{HHKW\_Wood\_max} * \text{HHKW\_Bin} - \text{HHKW\_Wood} \leq 1000. \tag{58}$$

The relationship between wood input and steam production is described by:

$$0 \leq -\text{HHKW\_Heat} + m_4 * \text{HHKW\_Wood} + n_4 * \text{HHKW\_Bin} \leq 0. \tag{59}$$

In accordance with the information provided in section 2.a, the steam generated from burning wood can be directed to either BPST *TG3* or ECST *TG2*. This condition is ensured by the following inequality:

$$0 \leq \text{HHKW\_TG3\_Bin} + \text{HHKW\_TG2\_Bin} \leq 1. \tag{60}$$

Therefore, we exclude the case where both binary variables are equal to 1.

The following balance equation ensures that the sum of HHKW_TG2_Heat and HHKW_TG3_Heat does not exceed total steam production HHKW_Heat:

$$0 \leq -\text{HHKW\_Heat} + \text{HHKW\_TG2\_Heat} + \text{HHKW\_TG3\_Heat} \leq 0. \tag{61}$$

The minimum and maximum steam transported to either *TG2* or *TG3* is limited by:

$$0 \leq \text{HHKW\_TG2\_Heat} - \text{HHKW\_Heat\_min} * \text{HHKW\_TG2\_Bin} \leq 1000, \tag{62}$$

$$0 \leq \text{HHKW\_Heat\_max} * \text{HHKW\_TG2\_Bin} - \text{HHKW\_TG2\_Heat} \leq 1000, \tag{63}$$

$$0 \leq \text{HHKW\_TG3\_Heat} - \text{HHKW\_Heat\_min} * \text{HHKW\_TG3\_Bin} \leq 1000, \tag{64}$$

$$0 \leq \text{HHKW\_Heat\_max} * \text{HHKW\_TG3\_Bin} - \text{HHKW\_TG3\_Heat} \leq 1000. \tag{65}$$

As a result, equation (60) to equation (65) enforce that total steam production HHKW_Heat must either be equal to HHKW_TG2_Heat or HHKW_TG3_Heat, and the latter should fall within the specified minimum and maximum bounds.

Assuming HHKW_TG3_Bin = 1, the relationship between steam input and power output through BPST *TG3* can be expressed as:

$$0 \leq -\text{TG3\_Power} + o_4 * \text{HHKW\_TG3\_Heat} + p_4 * \text{HHKW\_TG3\_Bin} \leq 0. \tag{66}$$

Similarly, the relationship between steam input and heat output through BPST *TG3* is given by:

$$0 \leq -\text{TG3\_Heat} + q_4 * \text{HHKW\_TG3\_Heat} + r_4 * \text{HHKW\_TG3\_Bin} \leq 0. \quad (67)$$

Therefore, equation (66) and equation (67) collectively represent the constant heat-to-power relationship described in section 2.e.2.

In the event that HHKW_TG2_Bin = 1 and/or GT_Bin = 1, we gather the steam produced by the wood-fired power plant, known as HHKW_TG2_Heat, and/or the HRSG, referred to as AHK_Heat, in a collector named Pre_TG2_Heat.

To ensure this, we maintain the following balance equation:

$$0 \leq \text{Pre\_TG2\_Heat} - \text{AHK\_Heat} - \text{HHKW\_TG2\_Heat} \leq 0. \quad (68)$$

The collected steam in the Pre_TG2_Heat collector has two options: it can either be directly sent as Heat_Extract to the district heating network, or it can pass as *TG2_Heat_in* through ECST *TG2*. This process is governed by the balance equation:

$$0 \leq \text{Heat\_Extract} + \text{TG2\_Heat\_in} - \text{Pre\_TG2\_Heat} \leq 0. \quad (69)$$

To restrict the extracted steam to its maximum capacity (33.14 MWth), we employ:

$$0 \leq \text{Heat\_Extract} \leq 33.14. \quad (70)$$

For *TG2* to be turned on, there are minimum and maximum steam input requirements. These conditions are described by:

$$0 \leq \text{TG2\_Heat\_in} - \text{TG2\_Heat\_in\_min} * \text{TG2\_Bin} \leq 1000, \quad (71)$$

$$0 \leq \text{TG2\_Heat\_in\_max} * \text{TG2\_Bin} - \text{TG2\_Heat\_in} \leq 1000. \quad (72)$$

In the same way, we model the FOR and the associated steam input (TG2_Heat_in) for ECST *TG2*.

At minimum steam input, power and heat can be converted as follows:

$$-1000 \leq -\text{TG2\_Power} + o_5 * \text{TG2\_Heat} + p_5 * \text{TG2\_Bin} \leq 0. \quad (73)$$

At maximum steam input, the power-to-heat conversion is given by:

$$0 \leq -\text{TG2\_Power} + q_5 * \text{TG2\_Heat} + r_5 * \text{TG2\_Bin} \leq 1000. \quad (74)$$

Figure 14 illustrates the lower and upper bound of *TG2*.

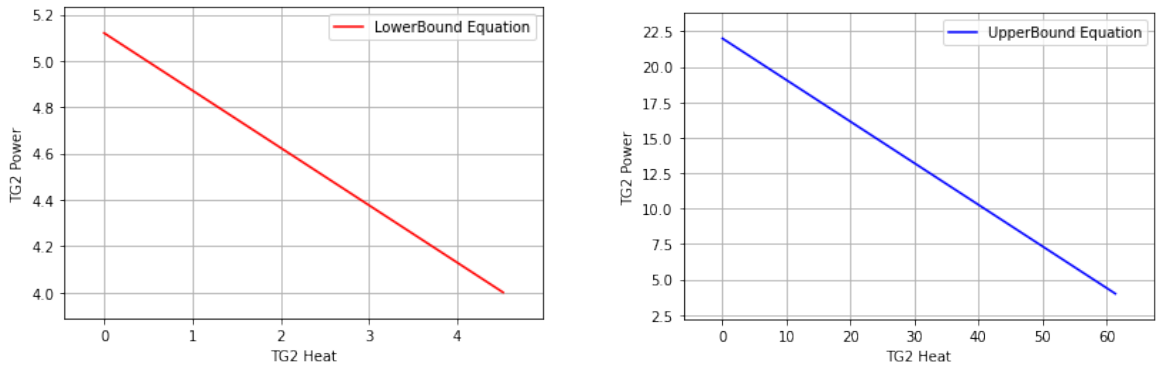

(a) Lower Bound Equation **(b)** Upper Bound Equation

Figure 14: Heat-to-power conversion via ECST *TG2* in MW

In order to establish the plane equation using the least-squares (LS) method in a three-dimensional space, we assign the y-axis to represent power output (TG2_Power), the x-axis to indicate steam input (TG2_Heat_in), and the z-axis to denote heat output (TG2_Heat).

The plane equation takes the form:

$$0 \leq -a_5 * \text{TG2\_Heat\_in} + b_5 * \text{TG2\_Power} + c_5 * \text{TG2\_Heat} + d_5 * \text{TG2\_Bin} \leq 0. \quad (75)$$

Figure 15 represents equation (75) graphically.

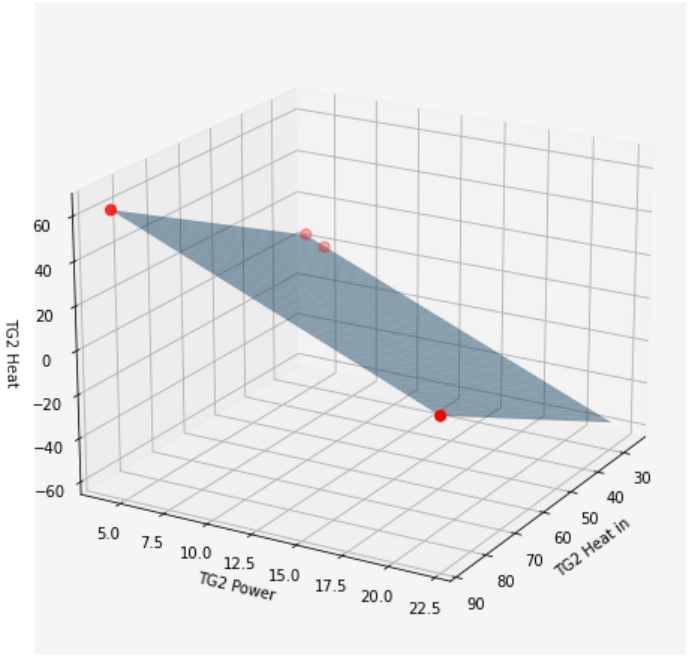

Figure 15: Plane equation of ECST *TG2* in MW

3.a.4. Ramping behavior of gas turbine (GT)

ewb is mandated to recycle all sweepings and accept a certain amount of wood. Hence, except for maintenance, the waster incinerator and wood-fired power plant operate continuously. Thus, we model ramps exclusively on the CCGT. Unlike the two other CHPs, the gas turbine (GT) offers greater flexibility for ramping up and down. We distinguish between two types of ramps: start-up and shut-down.

For that, we need to introduce the variable γ to disable the relationship between GT_Gas, GT_Power, AHK_Heat during the ramp process. We set γ arbitrarily high to 100.

Hence, we replace equation (55) by:

$$-\gamma \leq -\text{GT\_Power} + m * \text{GT\_Gas} + (n - \gamma) * \text{GT\_Bin} \leq 1000, \tag{76}$$

$$-1000 \leq -\text{GT\_Power} + m * \text{GT\_Gas} + (n + \gamma) * \text{GT\_Bin} \leq \gamma. \tag{77}$$

Similarly, we replace equation (56) by:

$$-\gamma \leq -\text{AHK\_Heat} + o * \text{GT\_Gas} + (p - \gamma) * \text{GT\_Bin} \leq 1000, \tag{78}$$

$$-1000 \leq -\text{AHK\_Heat} + o * \text{GT\_Gas} + (p + \gamma) * \text{GT\_Bin} \leq \gamma. \tag{79}$$

Hence, if GT_Bin $= 1$, we get the same relationship as in equation (55) and equation (56). However, if GT_Bin $= 0$, the relationship between GT_Gas and GT_Power/ AHK_Heat can vary between $-\gamma$ and γ. In this way, we implicitly substitute equation (53) and equation (54).

To ensure that the GT's power production in GT_Bin $= 0$ is not restricted to 0, we can use the following condition:

$$0 \leq \text{GT\_Pmax\_Inverse} * \text{GT\_Power} \leq 1. \tag{80}$$

GT_Pmax_Inverse is the inverse of GT's maximum power generation.

The specific gas consumption and corresponding power generation during ramp-up and ramp-down are presented in table 1.

Hours	Gas ramp-up	Power ramp-up	Gas ramp-down	Power ramp-down
0.00	40	5	80	30
1.00	80	30	0	0

Table 1: Ramping behavior of gas turbine

In a first run, we set the minimum up-time UT_3 to 24 hours, and the minimum down-time DT_3 to 1 hour. In a second run, we model more flexibility with $UT_3 = 6$ and $DT_3 = 1$. The hourly operational cost $c_{3,t}^{VOM}$ amount to EUR 140, and start-up costs c_3^{SU} to EUR 2160, as described in equation (6).

3.b. Assumptions

Due to time constraints and complexity, we made the following assumptions for our MILP-UC model:

1. We abstracted certain power plant components of the EZF, including the heat recovery, air condenser, air preheater and power-to-heat (P2H).

2. We neglected the unit's own electricity demands.

3. We did not explicitly account for the different pressure levels at which steam can be extracted or converted. For instance, figure 1 reveals that steam entering *TG1* can be extracted at either 3 or 12 bar. However, we combined them as KVA_Heat. Instead of modeling each steam pipe at its specific pressure level, we approximated the steam-to-heat and steam-to-power conversion. For that, we determined the specific enthalpy using the steam pressure and temperature. Next, we defined the power boundary points $ABCD$ for the feasible operation region (FOR) (in megawatts (MW)) on the minimum and maximum steam quantity.

4. We did not differentiate between process steam and district heating. Process steam is high-pressure steam (at 40 bar) sold to ewb's industrial consumers; namely ARA and Inotex. To address this, we would need to add yearly contracts representing the heat demand of industrial consumers to our UC problem. However, this would require to incorporate the different pressure levels explicitly.

5. We restricted our wood-fired power plant to choose either the steam turbine *TG2* or *TG3*. In our model, they cannot operate simultaneously when only waste and wood are burned. Though, in practice, the EZF's operator rarely used both steam turbines for wood burning during transitional periods (autumn and spring).

6. We restricted the HRSG's produced steam at 60 bar, AHK_Heat, to run via ECST *TG2*. In practice, it could also run via *TG3*.

7. We approximated the amount of waste in the bunker and its calorific value. In reality, the calorific value of waste varies over time. To partly compensate for that, we modeled the waste-to-steam efficiency around 0.85 instead of 0.89. Similarly, the calorific value of wood depends on the quality of the fresh and recycled wood used. Hence, we approximated the potential steam generation per megawatt burnt waste or wood.

8. We have not considered the additional waste heat, when the HRSG is used. The additional waste heat is of 2 megawatts.

9. We did not take into account that both KVA_Heat_Extract and Heat_Extract use the same steam line. To avoid exceeding the maximum capacity of this 40 bar line,

we should combine their capacities. This means treating the waste incinerator, the CCGT, and the wood-fired power plant as a single entity in TS-Energy.

10. We run our MILP-UC model twice: First, we restrict the GT's minimum up-time UT_3 to 24 hours, and the minimum down-time DT_3 to 1 hour. Moreover, we constrain our steam turbines *TG1*, *TG2* and *TG3* to run minimum 24 hours in a row. In the following, we refer to as "restricted model". These constraints are being implemented by the power plant operators at EZF. In a second run, we allow for more flexibility by setting $UT_3 = 6$ and $DT_3 = 1$, and removing the steam turbines' minimum up-times. Hereafter, we refer to as "flexible model".

4. Results

We compare the results of the restricted model with the actual data from the EZF over the year 2022. By doing so, we verify how effective our MILP-UC model is. Furthermore, section 4.b compares the restricted to the flexible model.

4.a. Effectiveness of proposed model

We present the results graphically for each CHP and heat-only unit k for the first two weeks and the last two weeks of December 2022.

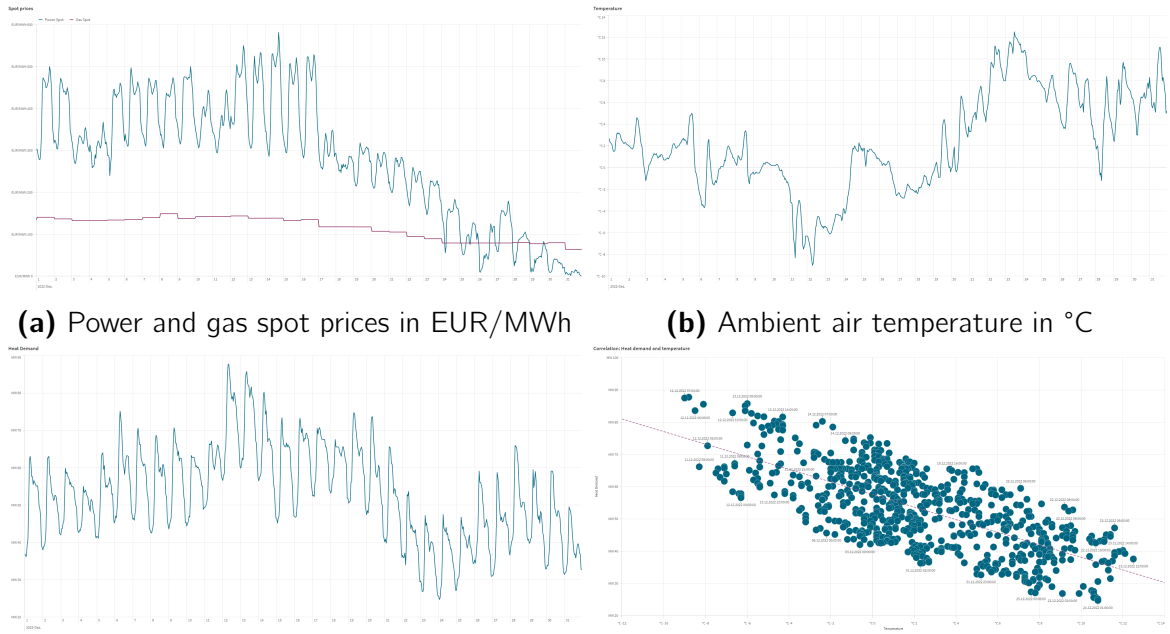

(a) Power and gas spot prices in EUR/MWh

(b) Ambient air temperature in °C

(c) Heat demand of the City of Bern in MW

(d) Correlation: heat demand and temperature

Figure 16: Exogenous drivers in December 2022

These time periods are particularly interesting for the following reasons: First, throughout 2022, the European energy crisis drove power prices to historically high levels (IEA, 2023). That is why we observe power spot prices of EUR 500 per megawatt hour in figure 16a. Second, figure 16a illustrates a usual power-price pattern for the last two weeks in a year: Power spot prices decrease due to simultaneous low energy demand and constant energy supply from base-load such as nuclear and possibly intermittent energy like wind. Low demand can be explained by holidays and reduced industry. Figure 16b illustrates daily heat demand. Heat demand exhibits distinctive fluctuations, with higher demand during the colder hours of the morning and evening. As the day progresses, heat demand

tends to decrease, reaching its lowest point during the late-night or early morning hours. The recurring pattern is influenced by weather conditions and human activity. Indeed, figure 16b indicates that after a brief cold spell until the 19th, a subsequent mild phase provided a surplus of 1 degree until the end of the month. As a result, the heat load has gradually fallen after the 19th, as shown in figure 16c. Figure 16d depicts the negative correlation between temperature (x-axis in °C) and heat load (y-axis in MW): The higher the temperature in winter, the less energy needed for heating.

Reduced industry activity leads to less waste available for the EZF. Particularly, as the EZF receives a lot of construction waste from Bern and its surroundings. The blue line in figure 17 reveals that the actual amount of waste burnt decreases gradually from 60 MWh to 40 MWh. On December 30, we observe a peak in the amount of waste incinerated, which has been stored in the bunker over Christmas holidays.

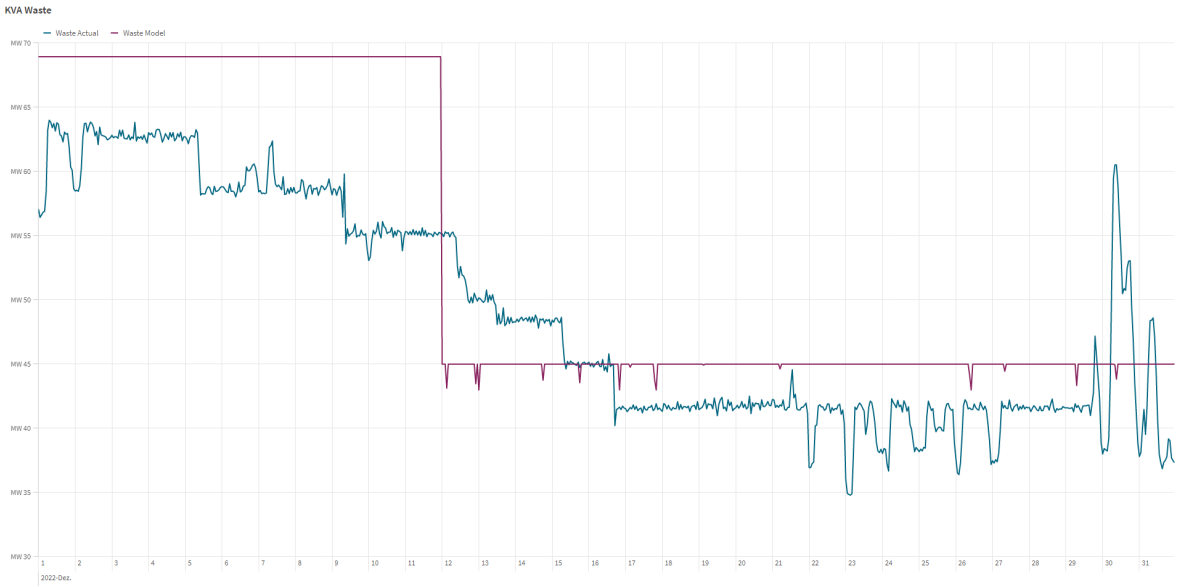

Figure 17: Waste consumption in MW: actual vs. model

4.a.1. Waste incinerator (KVA)

Figure 17 indicates that the actual calorific value of waste is lower than assumed. Indeed, compared to reality, our model has 15.9% more waste available in 2022. Consequently, we expect our model to have higher heat extraction or generate more heat and power via ECST *TG1*. In fact, our model generates 10% more power, while producing 5% less heat via *TG1* for the year 2022. However, as ewb is obliged to constantly provide process steam at 40 bar to ARA, the actual schedule's heat extraction (20'766 MWh) exceeds the model's heat extraction (7'847 MWh). Figure 18a illustrates this difference for December 2022: The actual schedule constantly extracts 5 MW steam at 40 bar.

In comparison to the waste incinerator's actual schedule (blue line), our model (red line) suggests a more frequent on-off pattern for ECST *TG1*, as shown in figure 18a. For instance, from December 19 to December 31, the model wants to turn off *TG1* eight times. This is shown for power in figure 18b and heat in figure 18c, respectively. The model's intuition is based on two factors: First, figure 16a shows close to zero power prices in this period. Second, according to equation (52), there is a minimum power output when steam enters *TG1*. Nevertheless, whenever our model turns off *TG1*, it has to extract all the resulting steam from mandatory waste burning, as shown in figure 18a.

To conclude, while the actual schedule constantly provides 5 MWh process steam, our model extracts heat alone in unfavorable power spot price situations or when heat is needed to satisfy heat demand. To ensure technical feasibility, we need to consult with the EZF's operators regarding the maximum heat extraction and the up and down drives of the latter. Besides the difference in waste input, these aspects represent the most significant differences between our model and the actual schedule.

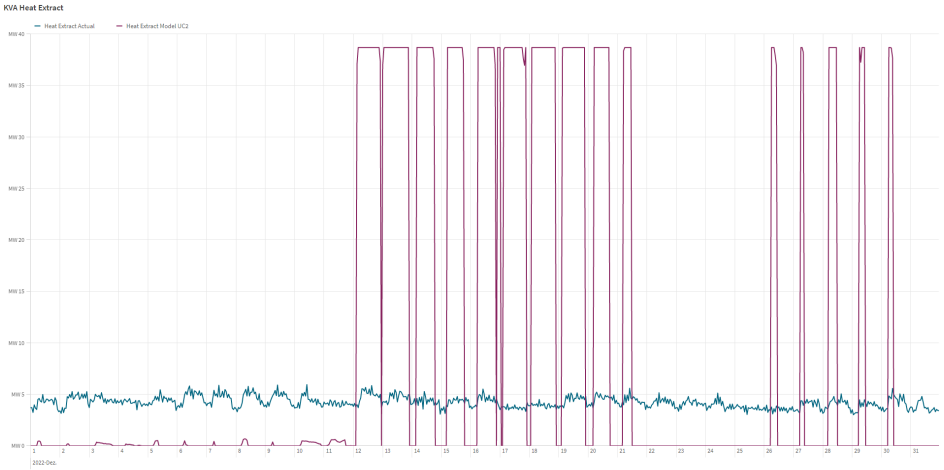

(a) KVA heat extraction in MW

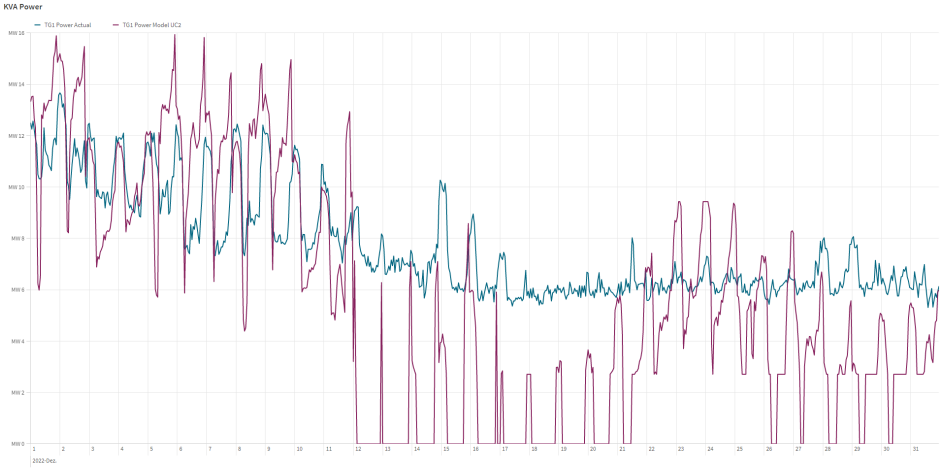

(b) KVA power generation in MW

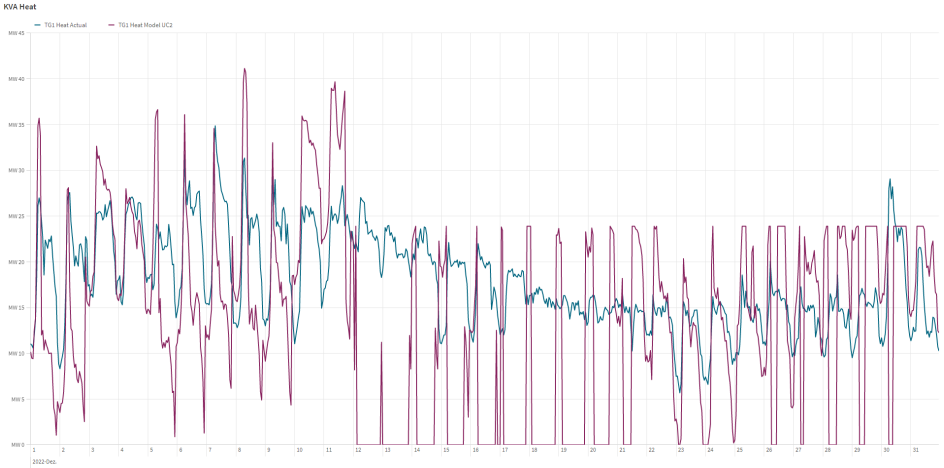

(c) KVA heat generation in MW

Figure 18: Waste incinerator: actual vs. model

4.a.2. Gas Turbine (GT)

In figure 19a, the red line demonstrates that the gas turbine's ramping behavior adheres to the model constraints defined in section 3.a.4. It meets the minimum-up and -down times and mimics the gas consumption and corresponding power generation during ramp-up and ramp-down. The red line also shows the temperature-dependent efficiency of the gas turbine, as governed in section 2.e.3. As the temperature rises during the day, gas intake, power, and heat generation decrease. In figure 19b, we observe how the HRSG's steam generation consistently relates to the power output. Notably, figure 19a reveals a small gap between the model and actual schedule at maximum gas consumption. This discrepancy can be attributed to our model's use of supplementary firing of the gas turbine, whereas the actual schedule rarely employs it.

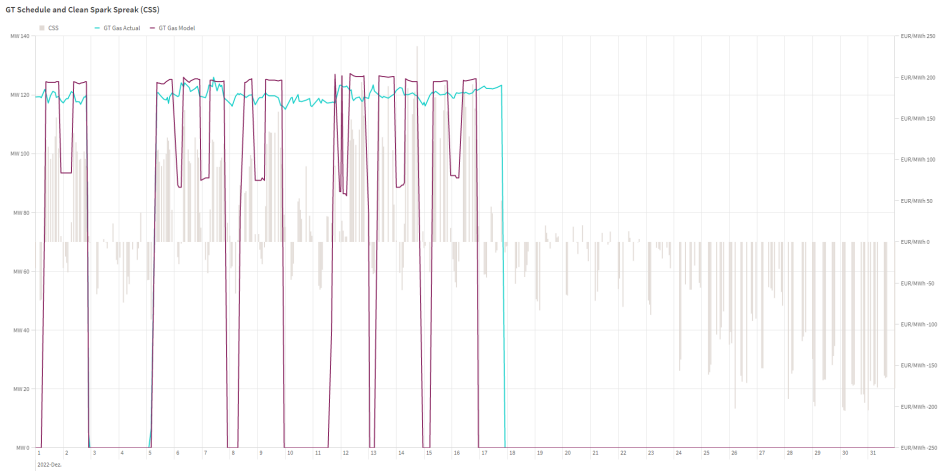

(a) CSS in EUR/MWh and GT gas consumption in MW

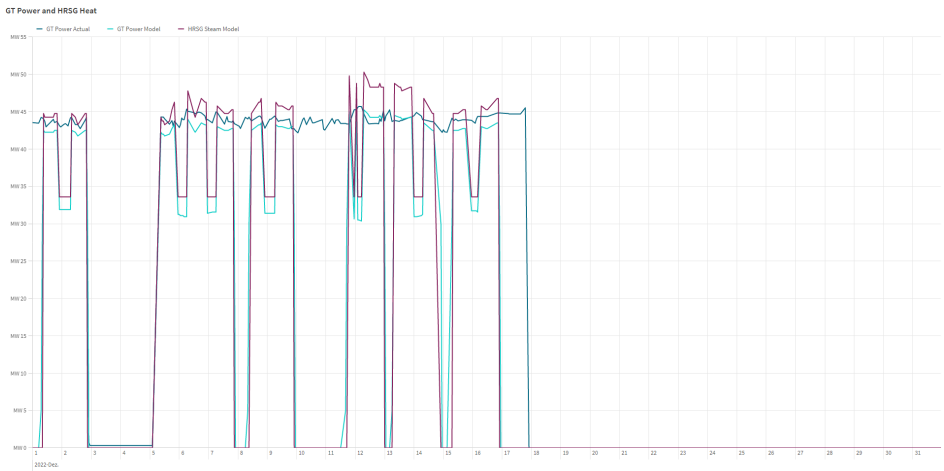

(b) GT power and HRSG heat generation in MW

Figure 19: CCGT: actual vs. model

As Switzerland is governed by the European Union Emissions Trading Scheme (EU ETS), ewb must consider the cost of the gas turbine's CO_2 emissions under this cap and trading regime. The so-called *clean spark spread (CSS)* represents the net revenue ewb makes from selling GT Power (turquoise line), having bought gas and the required number of carbon allowances (Bundesamt für Umwelt BAFU, 2023).
The clean spark spread is defined as follows:

$$\text{CSS} = \lambda_t^P - \frac{\lambda_t^G - 0.202 * \lambda_t^{CO_2,certificate}}{\eta_{el}}, \tag{81}$$

where η_{el} is the efficiency of power generation. In our case, η_{el} equals to 0.45. Hence, the CSS adjusts the cost of natural gas for the generation efficiency and the market cost of procuring or opportunity cost of setting aside an emissions allowance in the EU ETS (Zweifel et al., 2017). The bright bars in figure 19a illustrate the CSS for our gas turbine. A positive CSS indicates the profitability of operating the GT, whereas a negative CSS suggests otherwise.

Figure 19a compares the gas turbine's actual and model schedule: In reality, the gas turbine operated at maximum capacity non-stop from December 5 to December 18 (blue line). However, our model suggests four on/off cycles during that period (red line) and shuts down on December 17. According to our model, it is more cost-effective to shut down the GT for a few hours (at least 1 hour) despite high start-up costs. Figure 19a confirms that our model follows the CSS more accurately compared to the actual schedule. For instance, the model reduces load to 90 MW during off-peak hours at night. This is likely because power spot prices tend to decrease during that time due to lower energy demand.

4.a.3. CCGT (GuD) and wood-fired power plant (HHKW)

From figure 20, we can understand how the model operates the CCGT and the wood-fired power plant simultaneously. As mentioned in section 4.a.2, the gas turbine fluctuates several times, generating electricity (GT Power) and steam through the HRSG (HRSG Steam) until mid-December. Once the GT is on, the model decides to extract some of the collected steam directly as heat (Heat Extraction), as shown in figure 20b. The remaining steam powers ECST *TG2*. However, our model prioritizes power production if $CSS > 0$, resulting in practically zero heat generation (TG2 Heat) in December (see figure 20b).
Meanwhile, BPST *TG3* runs at maximum load with a constant power-to-heat ratio until December 25. After that, the model decides to shut down BPST *TG3* three times before the year ends. Instead, it extracts heat before *TG2* by using the generated steam from the wood-fired power plant. This happens when power spot prices approach the zero level, as illustrated in figure 16a.

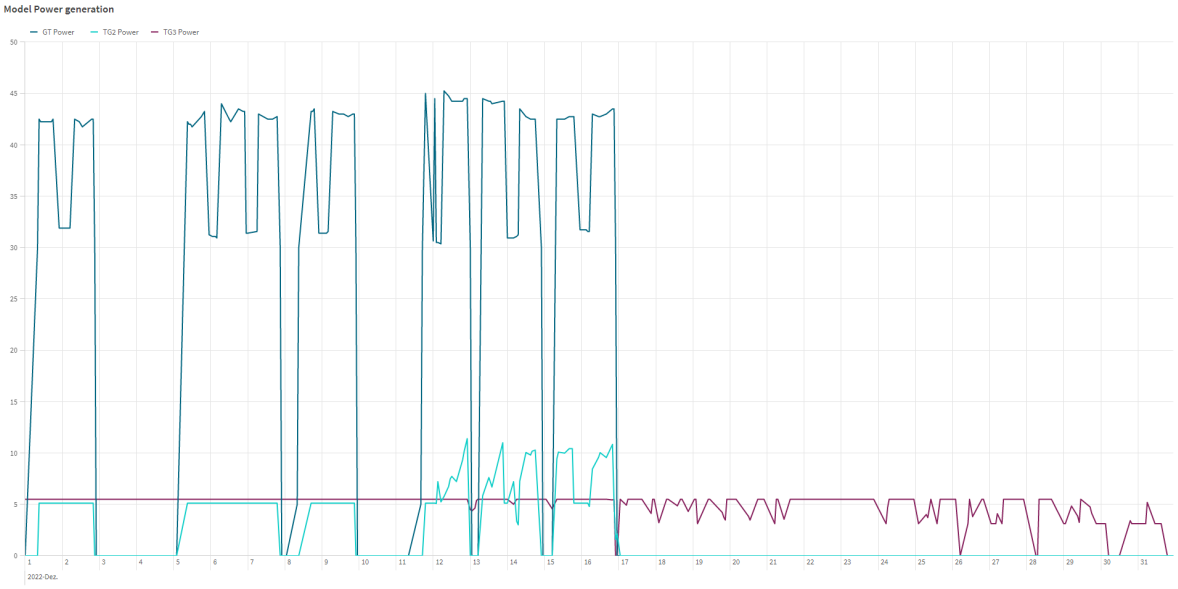

(a) *TG2* and *TG3* power generation in MW

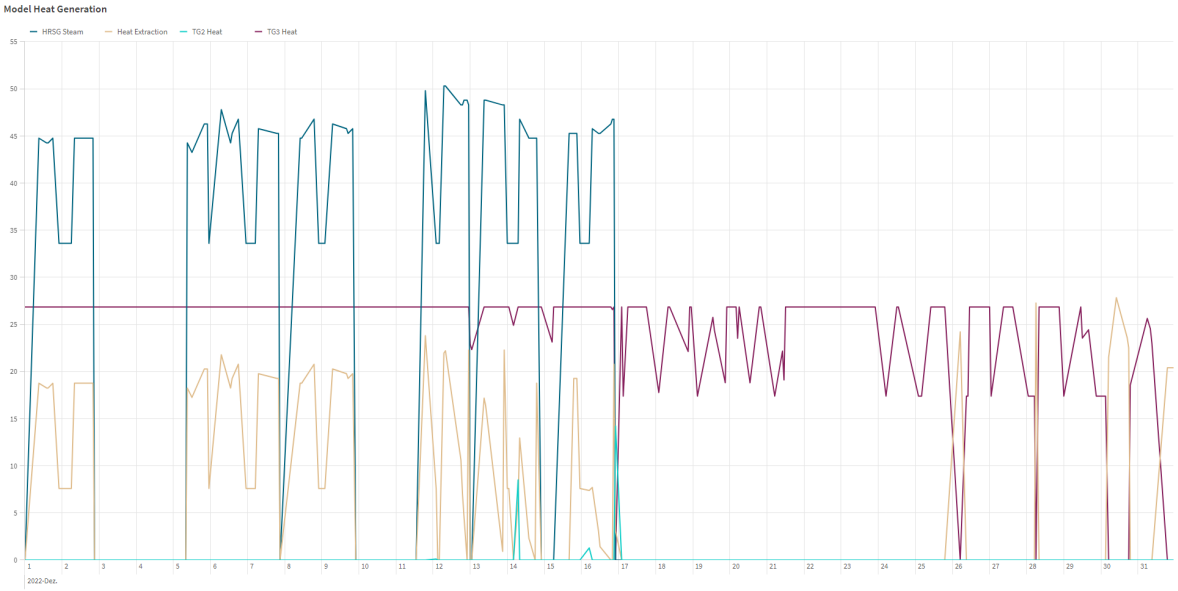

(b) *TG2* and *TG3* heat generation in MW

Figure 20: Model schedule in December 2022

Next, we want to compare the restricted model with the actual output from December 1 to December 19. To begin, figure 21 shows the actual and model wood consumption. The model initially burns wood at maximum load (37 MW) until December 13th. Afterwards, the model suggests reducing wood burning to a minimum load (24 MW), especially during nighttime. Yet, the blue line in figure 21 affirms that the actual calorific value of wood was lower than assumed: Our restricted model (296'350 MWh) consumes 16.2% more wood compared to the actual amount burned (255'083 MWh) throughout 2022.

Therefore, the assumption discussed in section 3.b becomes important. This variability is influenced by the quality of fresh and recycled wood delivered to ewb.

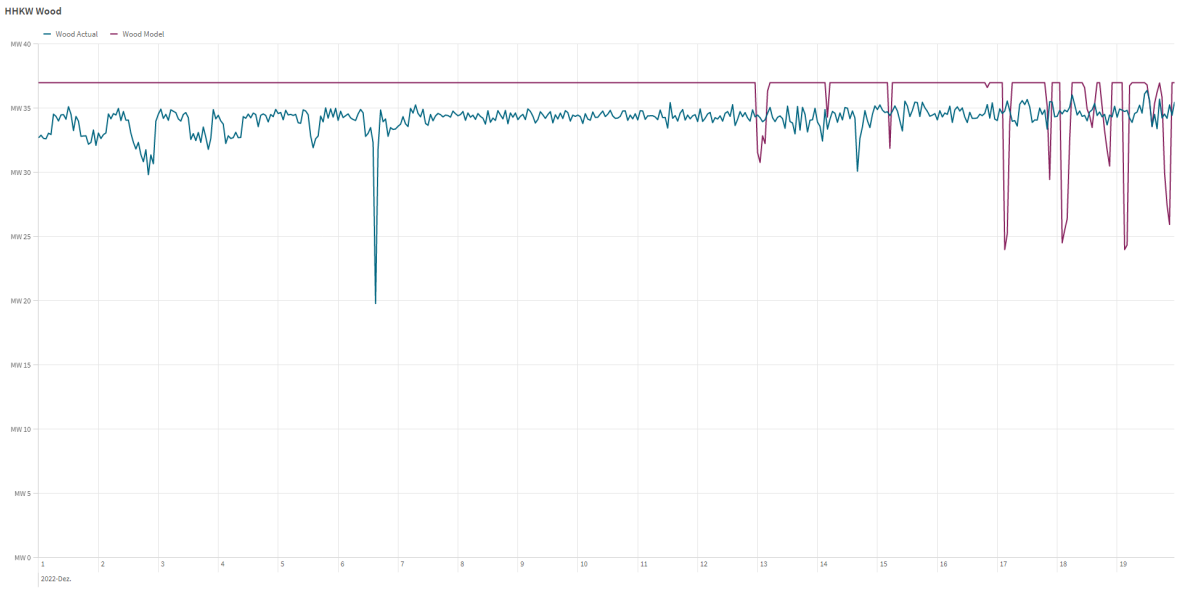

Figure 21: Wood consumption in MW: actual vs. model

Second, figure 22b indicates a significant discrepancy between the actual and model's power and heat output of ECST *TG2*. Whenever the CCGT was on, the actual schedule maximized *TG2*'s power production (blue line), while minimizing *TG2*'s heat generation (turquoise line) to zero. In addition, we observe in figure 22a that practically zero heat was extracted from wood and gas burning. According to equation (72), our model necessarily requires ECST *TG2* if the GT operates at maximum capacity. Opposed to reality, our model decides to extract some steam before *TG2*, as shown in figure 22a. Consequently, the potential TG2 power output (yelllow line) shifts downward.
Combining figure 22a and figure 16, we can deduce two correlations for our restricted model. First, a positive correlation between heat extraction and the daily heat demand pattern: Heat Extraction is increased when heat demand increases. From an efficiency point of view, this makes sense as we lose less energy if we decouple heat directly instead of generating it via a steam turbine with additional efficiency losses. Second, we observe a negative relationship between heat extraction and power spot prices. For instance, the model suggested cutting heat extraction between December 11 and 16 for the sake of increasing TG2 Power. This coincided with peak electricity prices of almost EUR 600 per megawatt hour.

Lastly, figure 22c shows that our model aligns well with the actual schedule for *TG3*, except for the switch from *TG3* to *TG2* on December 16. This indicates that we accurately captured the technical characteristics of BPST *TG3*. The variations in actual power and heat generation from *TG3* can be attributed to the varying calorific value of

the burnt wood. However, starting from December 17, the restricted model focuses on burning wood on a minimum load during off-peak hours. As a result, power and heat generation from *TG3* decrease simultaneously. This is due to the constant heat-to-power relationship inherited by *TG3*, as defined in section 2.e.2. Nevertheless, figure 22c reveals that in reality, this relationship is not as linear as our model assumes. Figure 22c reveals that the actual power and heat generation via *TG3* was not explicitly adjusted during off-peak hours between the min and max load. This adjustment becomes all the more relevant when electricity prices are heading towards zero.

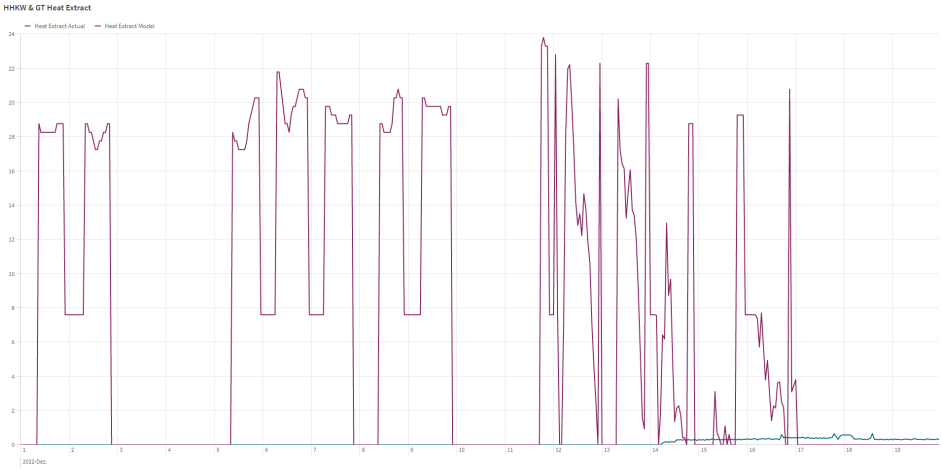

(a) Heat extraction of CCGT and wood-fired power plant in MW

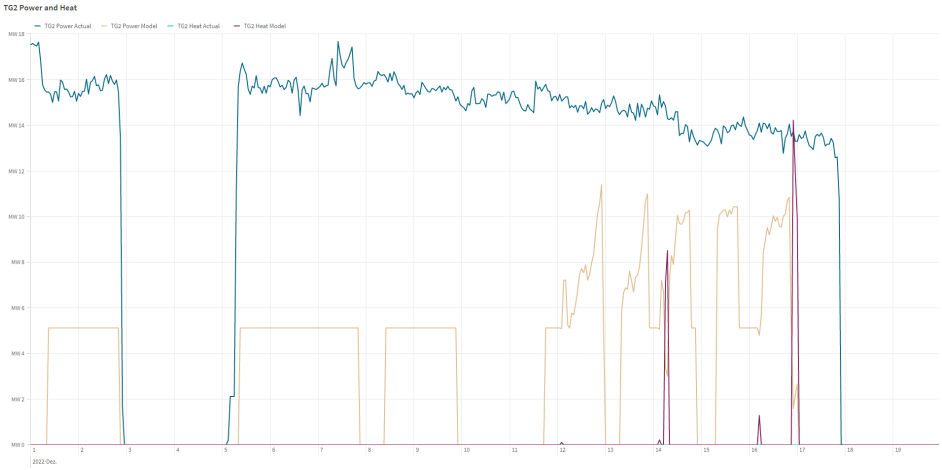

(b) TG2 power and heat generation in MW

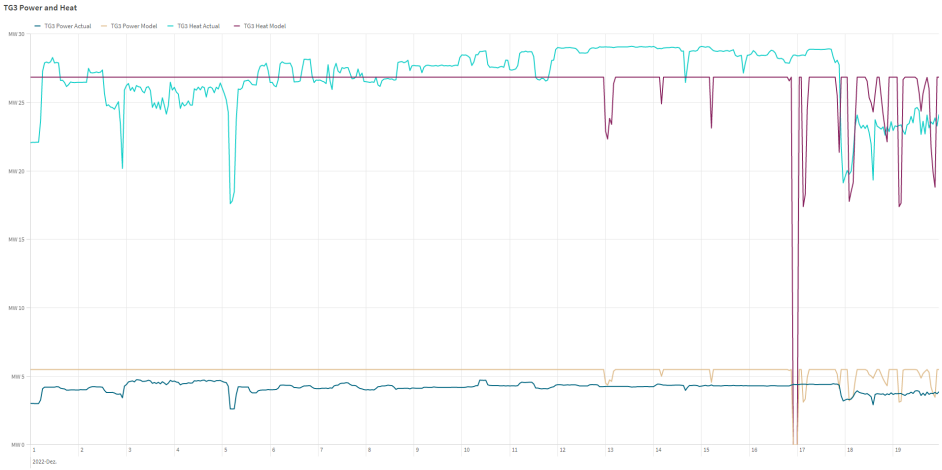

(c) TG3 power and heat generation in MW

Figure 22: Wood-fired power plant and CCGT: actual vs. model

4.a.4. Heat boiler (SLK)

The comparison of figure 23a and figure 23b shows that we have correctly modeled the machine characteristics and its efficiency under varying load, defined in section 2.d.6: The lower the load, the higher the efficiency losses during the gas-to-heat conversion. Figure 23 shows that our model operates the heat boiler less frequently during the period from 19 to 31 December 2022, compared to the actual schedule. This discrepancy will be later discussed in section 5.a. Figure 23b reveals a correlation between its heat generation and daily fluctuations in heat demand, a pattern observed in both the actual data and the model's output.

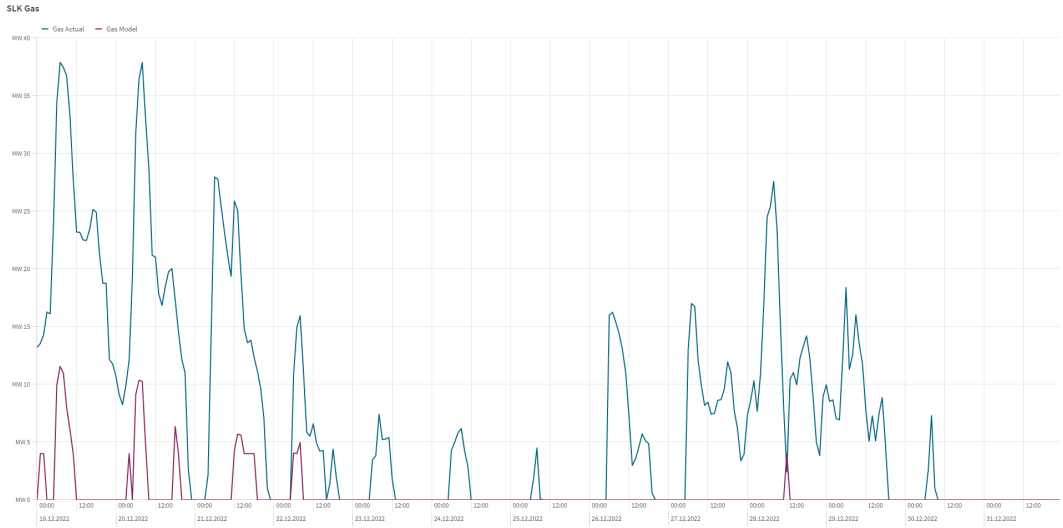

(a) Gas consumption in MW

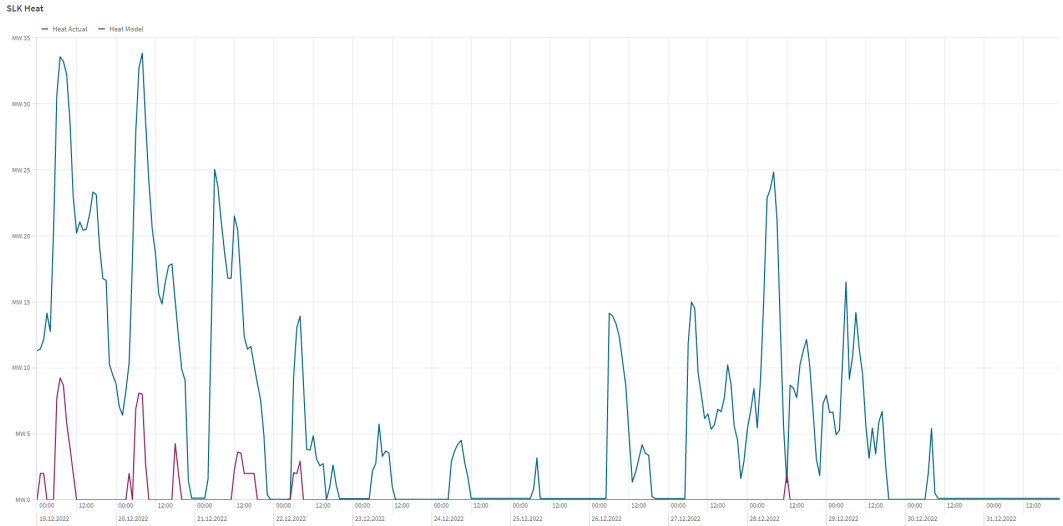

(b) Heat generation in MW

Figure 23: Heat boiler: actual vs. model

4.b. Model comparison

As mentioned in section 3.b, we allow the MILP-UC model to be more flexible in a second run: We set the GT's minimum up-time UT_3 to 6 hours and minimum down-time DT_3 to 1 hour. Additionally, we remove the steam turbines' minimum up-times. We compare the restricted model and the flexible model focusing on the schedules of the CCGT and the heat boiler, since the waste incinerator and wood-fired power plant schedules are nearly identical.

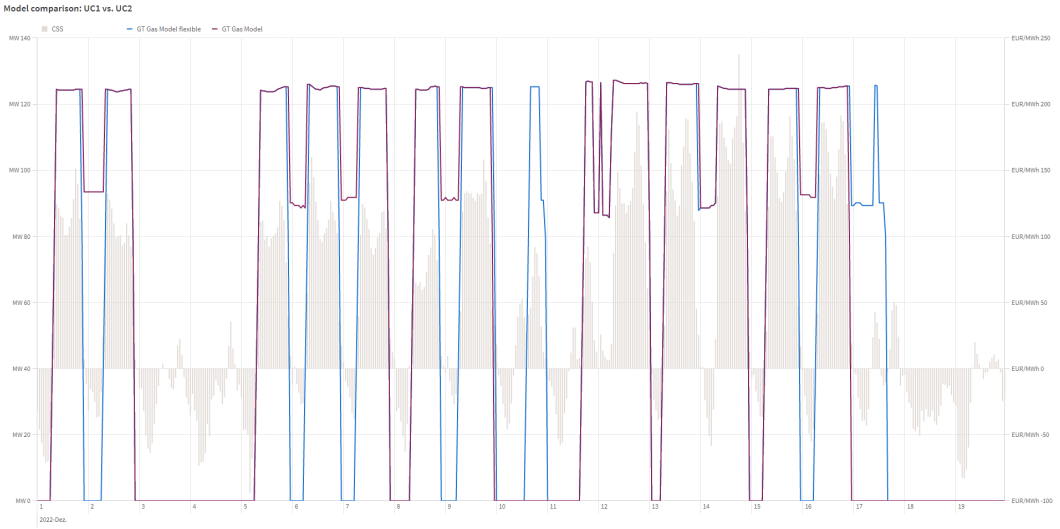

(a) GT gas consumption in MW and CSS in EUR/MWh

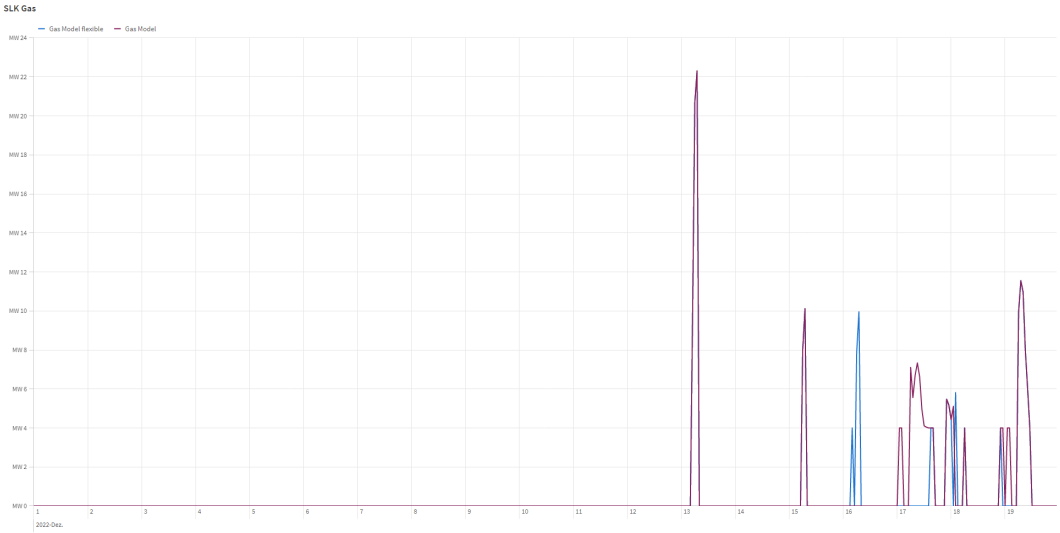

(b) Heat boiler gas consumption in MW

Figure 24: CCGT and heat boiler: model comparison

The blue line in figure 24a reveals that the gas turbine can follow the CSS more closely

in the flexible model. For instance, during the night of December 9, the flexible model decides to shut down the CCGT instead of reducing its minimum load of 90 MW (red line). The same can be observed for December 2, 6, 7, and 16 in figure 24. Interestingly, on December 17, the flexible model continues to operate the CCGT although CSS is negative until 7 pm, whereas the restricted model shuts down earlier. From 9 pm onward, the flexible model ramps up the CCGT to maximum gas consumption as the CSS becomes positive.

The schedule difference on December 17 could be explained by the flexible model preferring to produce heat via HRSG instead of the heat boiler. This is shown in figure 24b: With the exception of December 16, the flexible model (blue line) uses the heat boiler less for heat production than the restricted model (red line). This could indicate that the MILP-UC model even uses the gas turbine in a heat-led manner.

5. Discussion

In this section, we analyze the impact of the optimal heat and power output from section 4.a on the CO_2 balance. Further, we check the model for its profitability. Finally, we insert uncertainty into the model.

5.a. Analysis on CO2 balance

Figure 25 indicates that the gas turbine (311'990 MWh) and heat boiler (23'249 MWh) burnt in total 335'238 MWh gas in 2022. This gas amount released 67'718 tons of CO_2 emissions. In contrast, figure 25 reveals that our restricted model would have burnt in total 65'826 MWh gas: The heat boiler would have utilized 339 MWh of gas, while the gas turbine would have consumed 65'487 MWh of gas. This corresponds to 13'297 tons of CO_2. If we adopt the flexible model the heat boiler's gas consumption decreases by 22.4%, whereas the gas turbine's consumption rises by 10%, resulting in a 10% increase in CO_2 emissions. But since our model can generate additional 20'000 MWh heat from higher waste input, we do not account for the heat boiler's CO_2 emissions here. This assumption is reasonable because the difference between the heat boiler's actual and model's heat generation amounts to 19'643 MWh.

So, if the EZF had followed our restricted model's schedule, 45'028 tons of CO_2 emissions could have been avoided in 2022. Comparing the actual schedule with the flexible model, the difference is reduced by 4.3%. This amount equivalents to 150 million kilometers driven in a gasoline car or the annual CO_2 consumption of 3'200 people living in Switzerland (IEA, 2023).

Gas consumption in 2022: Actual vs. Model

Month	Heat boiler Actual	Heat boiler Model	Heat boiler Model flexible	GT Actual	GT Model	GT Model flexible
Total	**MWh 23'249**	**MWh 339**	**MWh 263**	**MWh 311'990**	**MWh 65'487**	**MWh 72'102**
Jan.	MWh 9'685	MWh 14	MWh 16	MWh 85'165	MWh 22'161	MWh 20'886
Feb.	MWh 1'756	MWh 0	MWh 0	MWh 76'589	MWh 0	MWh 0
März	MWh 2'745	MWh 0	MWh 0	MWh 52'135	MWh 0	MWh 4'992
Apr.	MWh 2'523	MWh 0	MWh 0	MWh 13'698	MWh 3'112	MWh 2'862
Mai	MWh 115	MWh 0	MWh 0	MWh 0	MWh 0	MWh 0
Juni	MWh 0	MWh 0	MWh 0	MWh 0	MWh 0	MWh 0
Juli	MWh 4	MWh 0	MWh 0	MWh 0	MWh 0	MWh 0
Aug.	MWh 538	MWh 0	MWh 0	MWh 0	MWh 0	MWh 0
Sep.	MWh 256	MWh 0	MWh 0	MWh 0	MWh 0	MWh 0
Okt.	MWh 597	MWh 0	MWh 0	MWh 1'000	MWh 1'074	MWh 2'006
Nov.	MWh 286	MWh 0	MWh 0	MWh 43'592	MWh 10'185	MWh 13'864
Dez.	MWh 4'744	MWh 325	MWh 248	MWh 39'809	MWh 28'955	MWh 27'492

Figure 25: Gas consumption in MW: actual vs. model

These findings support our hypothesis that an economically optimized scheduling of the EZF's energy production is also ecologically advantageous. Two main factors might contribute to this outcome: First, we expect the heat boiler only to be used if the CHP

units i cannot meet heat demand at time t. This is due to high input costs, including the gas spot price and and the Swiss tax on CO_2, and rather low payoff of EUR 36 per MWh. Besides, the gas-to-heat conversion process experiences an efficiency loss of 10%. Based on the results in section 4.a, we assume that our model prefers to extract steam before ECST *TG1* and *TG2*, even though it generates less power. Especially, when power spot prices approach the zero level. Consequently, we expect the heat boiler to be less frequently used to meet heat demand at time t and reduced gas consumption. To verify this hypothesis for *TG1*, we would need to run the model again applying the actual waste inputs. However, we know from section 4.a that our restricted model extracts 19'458 MWh more heat before *TG2* compared to the actual schedule.

Second, although the restricted model and the actual state of the EZF share the same minimum up- and down-time constraints for the GT, the model runs the CCGT less frequently. In other words, based on economics alone, the GT was used less in both models as it follows the CCS more closely. However, if we provide the model with more flexibility by reducing the GT's minimum up- and down-times, two opposing effects on gas consumption emerge: On the one hand, instead of reducing GT's gas consumption to a minimum during nighttime, the flexible model is able to completely shut down, reducing gas consumption. On the other hand, as the GT is not restricted to run 24 hours in a row, the flexible model might introduce additional ramp-up and -down phases, increasing gas consumption. In 2022, the second effect outweighed the first.

In summary, this ex-post analysis on the CO_2 balance validates the potential for reducing CO_2 emissions by optimizing the EZF based on hourly gas and power spot prices. However, for a short-term ex-ante scheduling problem, one is exposed to the uncertainty of the future development of spot prices.

5.b. Profitability analysis

Figure 26 summarizes total costs, the heat and power revenue and total profit for the year 2022. The results of the restricted model are compared with the actual schedule.

The key findings from figure 26 are as follows: First, our restricted MILP-UC model generates 13.7% more profit compared to the actual schedule. Because we have set the optimality gap to 1%, our confidence interval ranges from EUR 57.5 million to EUR 58.6 million. However, this difference might be due to the fact that our model assumes higher calorific values for wood and waste, resulting in lower heat production costs (see section 3.b). These renewables are the most cost-effective or even revenue-generating energy sources compared to gas, despite one exception: The gas spot price was lower than the wood price from October 22 to November 2, 2022. Hence, we expect our MILP-UC to prioritize renewable energy sources to satisfy heat demand solely from an economic perspective. In fact, whereas the actual schedule incurred EUR 32 million in

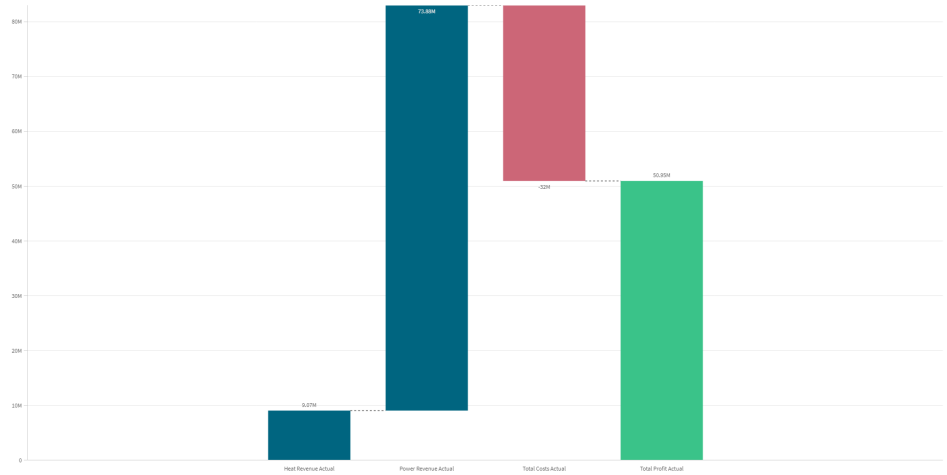

(a) Actual profitability in million EUR

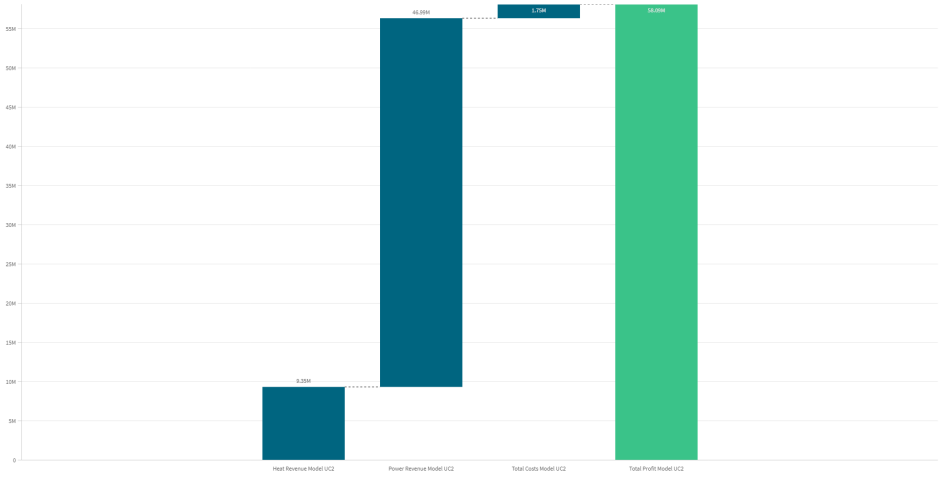

(b) Model profitability in million EUR

Figure 26: Profitability analysis in 2022: actual vs. restricted model

cost, our model shows negative costs of EUR -1.75 million for the year 2022. Besides the argument above, this variance can be attributed to our model's lower gas consumption, shown in figure 25. Second, our MILP model generates about the same heat revenue for the year 2022. On the contrary, our model earned 36.4% less profit from power generation. On the one hand, this variation is related to the actual schedule's higher GT power production, particularly evident from January to April: Compared to reality, our model earned 74.1% less from selling power generated by the gas turbine. On the other hand, based on the information from figure 20, our model prioritizes heat extraction, even if it means producing less power, especially when power prices are not favorable. This could partly explain the remaining difference between the actual and the model's power revenue. Notably, December 2022 is the only month where our MILP-UC model performs worse than the actual schedule. This difference might come from inaccurate

modelling of the technical characteristics of *TG2*.

In a second step, we examine how additional model flexibility influences profitability. First, the waste and wood consumption do not have an impact on profitability as they are the same in both models. Second, as the flexible model consumes more gas, we face an 8.1% increase in gas and CO_2 costs. However, the negative impact on the CO_2 balance is offset by a 1.5% boost in overall profit. Precisely, we can affirm that the flexible model was in each month more profitable compared to the restricted model. The increase in profit might come from selling more GT power to the spot market, reducing gas consumption when the CSS is slightly negative or operating the steam turbines more flexible, and thus, be able to switch faster from extraction to generation mode. This assumption aligns with the values in figure 27: While the flexible model saw a modest 0.3% increase in heat revenue, a remarkable 3.1% surge in power revenue becomes evident. Yet, attaining this enhanced flexibility entails the trade-off of recruiting extra staff at the EZF, given that the thermal system is coupled via heat recovery steam generation to the gas turbine. Skilled personnel are required to balance the rapid ramping up and down of the gas turbine within the thermal system.

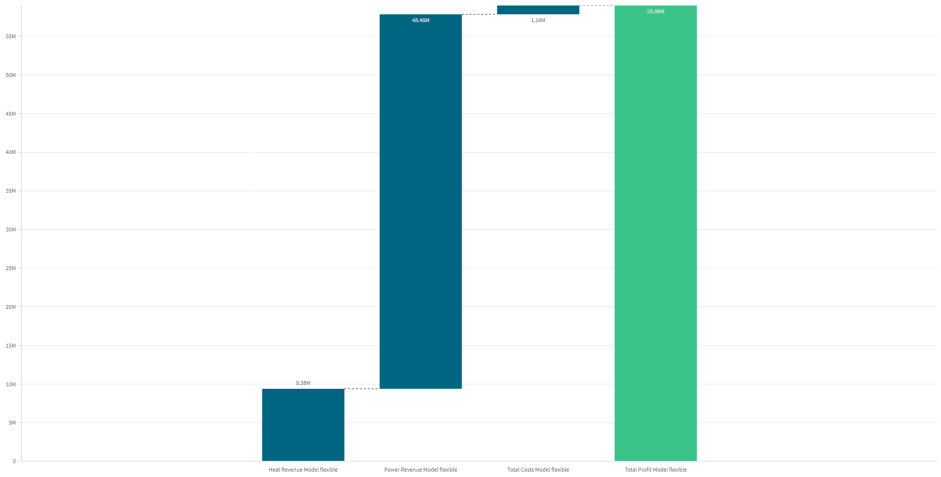

Figure 27: Profitability analysis in 2022 in million EUR: flexible model

5.c. Sensitivity analysis

We employ a linear regression model to assess the sensitivity of the power spot price and the gas spot price on the profit output of our restricted model. The linear regression equation can be expressed as:

$$Y_t = \beta_0 + \beta_1 X_{t,\text{power}} + \beta_2 X_{t,\text{gas}} + \varepsilon_t, \tag{82}$$

where Y_t is the predicted profit output, $X_{t,\text{power}}$ represents the power and $X_{t,\text{gas}}$ the gas spot price at hour t. β_0 is the intercept, and β_1 and β_2 are the coefficients associated with the power spot price and gas spot price, respectively. ε_t accounts for the error term.

For that, we gather historical market spot prices spanning from 2017 to 2021 and execute the restricted model on four separate occasions. The remarkable trajectory of power and gas spot prices is depicted in figure 28. Notably, our reference year 2022, marked by the red line, stands out as an outlier due to its substantial price level.

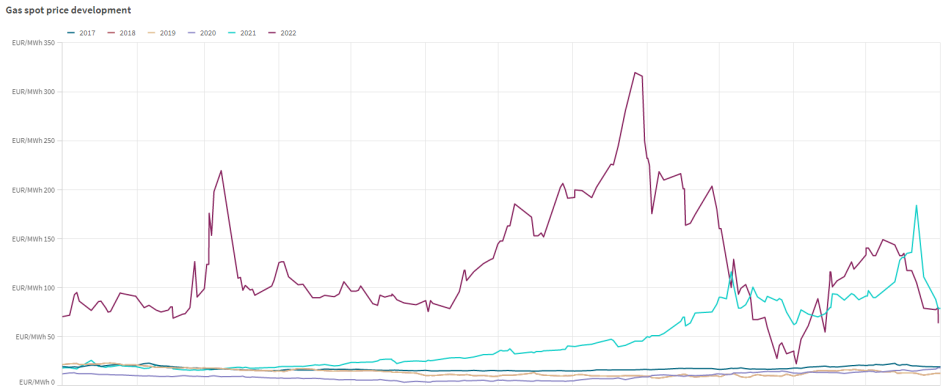

(a) Gas spot price in EUR/MWh

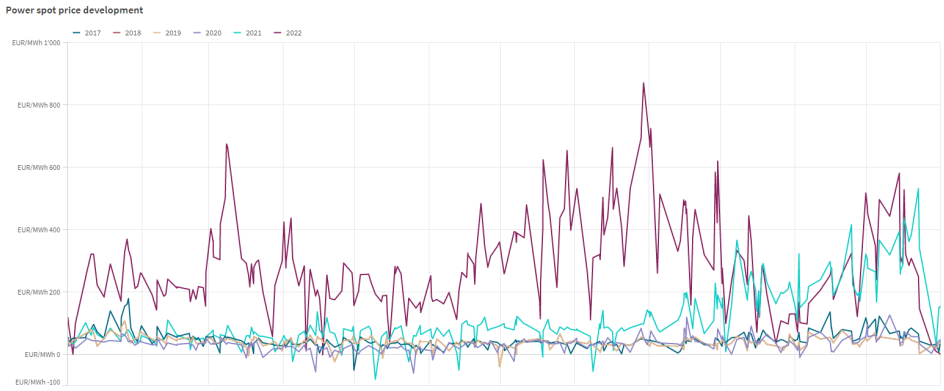

(b) Power spot price in EUR/MWh

Figure 28: Spot price development from 2017-2022

Table 2 summarizes the regression findings. β_1 and β_2 represent the first derivatives of the dependent variable with respect to the independent variable. Essentially, the coefficients quantify the rate of change in profit for a unit change in either gas or power price, while holding all other model variables constant. Hence, β_1 and β_2 offer a direct measure of the sensitivity of the EZF's profit to changes in the power or gas spot prices.

Table 2: Sensitivity analysis

	Estimate	Std. Error	t value	Pr(>|t|)
β_0	2705.3421	10.4730	258.32	0.0000
β_1	17.9381	0.1974	90.85	0.0000
β_2	-12.8346	0.4622	-27.77	0.0000

The estimated intercept β_0 is 2705, suggesting that when both the power spot and gas spot price are zero, the expected profit is EUR 2705. β_1 is 17.9, denoting that a single-unit increment in power spot price corresponds to an average gain of EUR 17.9 in profit, ceteris paribus. Unlike, a singe-unit increase in gas spot price decreases on average profit by EUR 12.8, holding everything else constant. The F-statistic (16'490) tests whether there is a significant linear relationship between the dependent variable and the independent variables. The associated p-value, being smaller than 2.2^{-16} indicates that the model is statistically significant.

These results align with our expectations: The negative input price of waste might explain positive profit although assuming the independent variables to be zero. Indeed, compared to our reference year 2022 we do not observe any changes in the waste incinerator's operation over the five model runs. This is potentially because the model always makes profit when processing waste. Second, an increase in the gas input price leads to a smaller clean spark spread (CSS), resulting in less utilization of the gas turbine, which significantly lowers profitability. On the contrary, when the power spot price rises, the CSS becomes larger, leading to increased operation of the gas turbine. We can infer that the CCGT is the most price sensitive power plant component of the EZF. Interestingly, when applying lower market prices (2017-2020), the heat boiler is more frequently used compared to 2021 and 2022. This might be because, due to the small CSS, the gas turbine operates less, resulting in less steam production that needs to be compensated for by the heat boiler. Similarly, when taking into account market prices from 2017-2020, the model utilized on average 225'000 MWh of wood. However, with our base year set as 2022, its consumption increased by 30%, resulting in higher power production.

It is important to acknowledge the limitations of our sensitivity analysis. To start, assuming a linear relationship between the independent and dependent variables may not accurately capture the underlying dynamics. Second, we might face the problem of multicollinearity as the gas price frequently sets the price at which electricity is sold

following the merit order (see appendix D) (Zweifel et al., 2017). This can make it difficult to interpret the individual coefficient effects. Third, we might face omitted variable bias by only incorporating two independent variable. For further studies, heat demand, being negatively correlated to temperature, should be considered as additional independent variable. This is because heat and power outputs of the CHP units are non-separable. Moreover, we anticipate a correlation between the gas spot price and the price for CO_2 certificates: For instance, if carbon prices increase due to stricter climate change policies, the European market favours gas over coal. In addition, the spread between the coal-to-gas switching price and the gas spot price sets the extent of the inter-fuel switching. If the spread is large, gas demand increases along with higher carbon prices (Singh, 2023; Zweifel et al., 2017).

To sum up, we potentially deviate from the assumption of linearity, and grapple with omitted variables bias as well as multicollinearity. We have explicitly refrained from undertaking an extensive sensitivity analysis, as our primary focus lies first in refining the precision of our model. However, for further exploration, we propose adopting a scenario-based sensitivity analysis. This approach would evaluate the influence of uncertain fuel prices, demand fluctuations and market conditions on the optimal power and heat output of the MILP-UC model. To execute this, we would define a set of scenarios, encompassing a span of potential values for each risk variable (gas spot price, power spot price and heat demand). Subsequently, we would solve the MILP-UC model and examine how solutions vary across these scenarios. By doing so, we could identify strategies that remain robust across multiple scenarios.

6. Conclusion

To achieve decarbonization targets, the energy sector needs to prioritize improving its efficiency and integrating renewable energy. However, with increasing penetration of renewables, power prices become highly volatile and more frequent generation-load imbalance may occur. Among other, combined heat and power (CHP) plants offer a solution to this conflict: First, CHPs achieve efficiency gains through the coupling of heat and power generation, that result in reduced carbon emissions. Second, a coordinated utilization of CHP units together with a district heating network can help to reduce the renewable curtailment and more cost-effective operation. This is precisely why achieving optimal operation of the Energiezentrale Forsthaus (EZF) is of outmost importance. The EZF combines three CHP units: namely, a waste incinerator, a wood-fired power plant and a combined-cycle gas turbine (CCGT) as well as a heat boiler. The EZF is connected to the district heating network and must constantly satisfy the city's heat demand. In contrast, its power production is secondary and can be economically optimized. Since the power and heat production are dependent on each other, the EZF offers a constrained arbitrage opportunity among generating heat and power.

Considering the need to align our generation schedule with heat demand and technical constraints such as minimum up/ down-time, capacity limits, ramp rates, unit availability, and fuel characteristics, most authors suggest using unit commitment (UC). This approach is widely recommended for efficiently managing the short-term scheduling of a CHP system like the EZF, particularly when considering the complexities of managing multiple generation units over time (Anand et al., 2018; Arroyo & Conejo, 2004; Morales-España et al., 2013; Nicolosi et al., 2021). By depicting the CHPs feasible operation regions (FOR) as convex regions, we capture their nonlinear efficiencies (Makkonen & Lahdelma, 2006). In short, greater loads and increased heat generation within the FOR lead to higher efficiency per megawatt of output.

We have chosen to solve our UC problem by Mixed Integer Linear Programming (MILP) because we consider a rather large deterministic model and want to find a solution that is a global optimum. Additionally, MILP allows us to easily linearize non-linear constraints (Chang et al., 2004; Kim & Edgar, 2014; Morales-España et al., 2013; C. Wang et al., 2022). We implemented the MILP-UC model in TS-Energy and used Fico Xpress optimizer to solve it. The optimality gap was set to 0.01. The computational time, required for a full year, took 35 minutes, a duration we consider reasonable.

We verified how effective our MILP-UC model is by comparing both graphically and quantitatively the model's optimal heat and power mix with the actual EZF data in 2022. First, our model was able to fulfill the unit commitment problem throughout the year. The model's total power and heat production were comparable to the actual output. This suggests that we have accurately modeled the units efficiencies and technical constraints. For instance, *TG3* was only prioritized over *TG2* during the winter months,

when the heat, resulting from the constant power-to-heat ratio of a backpressure steam turbine, could be effectively used. Nevertheless, while ewb operated both ECST *TG1* and *TG2* with a more or less steady power and heat production, our MILP-UC model proposes a more frequent on-and-off pattern. Precisely, our model often extracts heat before steam entering *TG1* or *TG2* for the sake of producing less power. This can be observed when power spot prices are low.

We have identified significant potential for reducing CO_2 emissions: Adhering to our restricted model's schedule could have prevented 45'028 tons of CO_2 emissions in 2022. These findings strongly support our hypothesis that an economically optimized scheduling of the EZF's energy production is also ecologically advantageous. There are two possible explanations for that: First, we expect the heat boiler to be less frequently used due to enhanced heat extraction and hence, reduced gas consumption. Second, the model runs the CCGT less frequently based on economic grounds alone as it follows the clean spark spread (CSS) more accurately.

Next, our MILP-UC model has proven to be highly profitable, outperforming the annual EZF profit by 13.7%. Further, we can infer that additional model flexibility has led to 3.1% increased profit. Yet, this flexibility comes with the opportunity cost of having a negative effect on the CO_2 balance and hiring additional staff at ewb. Last but not least, we employed a linear regression model to assess the sensitivity of the gas and power prices on our model's profitability. For that, we inserted historical market spot prices from 2017 to 2021. The linear regression model suggests that both power and gas spot prices are statistically significant predictors of profit: While a one-unit increase in gas spot price lowers profitability by 12.8 EUR, a one-euro increase in power spot price raises profit by EUR 17.9, ceteris paribus. Moreover, from graphical inference we can confirm that our model stays robust in its operation. This is especially true for the waste incinerator and the wood-fired power plant. However, the heat boiler and the CCGT are the most flexible units inside the EZF and strontly react to short-term price fluctuations. In sum, the EZF's annual profit is highly sensitive to changes in power and gas spot prices due to the CCGT, but will never be negative thanks to the revenue generated by waste processing.

In essence, we established a MILP-UC model to find hourly optimal power and heat production for the EZF, ensuring heat demand is met. The expected effects were to enhance efficiency through optimal capacity usage, enable responsiveness to short-term power price fluctuations, and ultimately to cut on CO_2 emissions. Imaging results revealed potential gains in profitability alongside a notable decrease in CO_2 emissions.

However, the present MILP-UC model has several limitations that require discussion. First, we overestimated the calorific value of waste and wood. This resulted in increased model profitability and potentially reduced gas consumption by the heat boiler. Accordingly, we had to adjust our analysis on the CO_2 balance. For simplicity, we abstracted certain power plant components as well as some steam lines of the EZF. Further, we

did not account for the different pressure levels at which steam can be extracted or converted. As a result, we did not differentiate between process steam and district heating, which present in reality separate contracts to be fulfilled by the EZF. Instead, we approximated the steam-to-heat and steam-to-power conversions for *TG1* and *TG2*. Hence, we do anticipate some inaccuracies in the technical constraints, precisely in defining the feasible operation regions of the CHP units.

Future research could repeat a model run with the 2022's actual waste input and check the model's profitability again. Next, we could discuss with the EZF's operators if the proposed schedule with increased heat extraction and more frequent on-and-off patterns of the steam turbines is technically feasible. If so, we propose to enhance model complexity by applying some of the simplifications described in section 3.b. To apply the MILP-UC model as short-term scheduling tool requires daily or weekly forecasts of heat load as well as of power and gas spot prices. So, the EZF operator could respond to the significant power price fluctuations that arise due to intermittent renewable energy sources. Furthermore, a scenario-based sensitivity analysis could help in strategic decision making. Precisely, we suggest considering heat demand, power and gas spot prices as risk variables and examine how sensitive the model's optimal day-ahead operation is to these uncertainties.

There are some exciting applications for model extensions thanks to ewb's investment projects: First, ewb is currently developing a seasonal heat storage with 12 GWh capacity. The "Geospeicher" works by utilizing underground reservoirs of porous rock formations to store the EZF's excess energy (during summer) in the form of heat and then release it when demand is high. In the winter months, the stored heat can be extracted and fed into the district heating network or used for power generation (Energie Wasser Bern, 2023). By including the "Geospeicher" as additional model entity in TS-Energy, we expect increased model flexibility as further decoupling between heat and power generation becomes possible. This may help the EZF to change capacity when power prices are preferable and thus, increase profits. Second, ewb is building additional CHPs, including a wood-fired power plant, geothermal probe and photovoltaics that should cover the district heating expansion in the city of Bern. As those CHPs are connected to the EZF's district heating network, our MILP-UC model could predict from which source the cheapest and most efficient heat could be generated at hour t. Besides the planned projects, we encourage ewb to invest in better quality wood to increase the wood-fired power plant's efficiency. Last but not least, we propose to run the gas turbine on a renewable energy source such as biomass to reconcile the city's climate goals with the EZF's energy production. However, considering the higher cost of biogas production, profitability would need to be re-evaluated.

References

Aghaei, J., & Alizadeh, M.-I. (2013). Multi-objective self-scheduling of chp (combined heat and power)-based microgrids considering demand response programs and esss (energy storage systems). *Energy*, *55*, 1044–1054.

Algie, C., & Wong, K. (2002). Reduced cogeneration feasible operating region for combined heat and power scheduling problems, 323–328. https://doi.org/10.1049/cp:20020056

Alipour, M., Zare, K., & Mohammadi-ivatloo, B. (2014). Short-term scheduling of combined heat and power generation units in the presence of demand response programs. *Energy*, *71*. https://doi.org/10.1016/j.energy.2014.04.059

Anand, H., Narang, N., & Dhillon, J. (2018). Unit commitment considering dual-mode combined heat and power generating units using integrated optimization technique. *Energy Conversion and Management*, *171*. https://doi.org/10.1016/j.enconman.2018.06.054

Arroyo, J., & Conejo, A. (2004). Modeling of start-up and shut-down power trajectories of thermal units. *Power Systems, IEEE Transactions on*, *19*, 1562–1568. https://doi.org/10.1109/TPWRS.2004.831654

Benichou, M., Gauthier, J. M., Girodet, P., Hentges, G., Ribiere, G., & Vincent, O. (1971). Experiments in mixed-integer linear programming. *Mathematical Programming*, *1*(1), 76–94.

Carrion, M., & Arroyo, J. (2006). A computationally efficient mixed-integer linear formulation for the thermal unit commitment problem. *Power Systems, IEEE Transactions on*, *21*, 1371–1378. https://doi.org/10.1109/TPWRS.2006.876672

Chang, G., Tsai, Y., Lai, C., & Chung, J. (2004). A practical mixed integer linear programming based approach for unit commitment. *2004 IEEE Power Engineering Society General Meeting*, *1*, 221–225 Vol.1. https://doi.org/10.1109/PES.2004.1372789

Dakin, R. J. (1965). A tree-search algorithm for mixed integer programming problems. *The Computer Journal*, *8*(3), 250–255.

Elfarra, M., & Kaya, M. (2018). Comparison of optimum spline-based probability density functions to parametric distributions for the wind speed data in terms of annual energy production. *Energies*, *11*, 3190. https://doi.org/10.3390/en11113190

González-Díaz, A., Alcaráz-Calderón, A. M., González-Díaz, M. O., Méndez-Aranda, Á., Lucquiaud, M., & González-Santaló, J. M. (2017). Effect of the ambient conditions on gas turbine combined cycle power plants with post-combustion co2 capture. *Energy*, *134*, 221–233.

IEA. (2023). *Co2 emissions in 2022*. https://www.iea.org/reports/co2-emissions-in-2022

Jimenez Navarro, J., Zucker, A., Quoilin, S., & Kavvadias, K. (2018). *Case study on the impact of cogeneration and thermal storage on the flexibility of the power system*. European Commission; Joint Research Centre.

Kim, J. S., & Edgar, T. F. (2014). Optimal scheduling of combined heat and power plants using mixed-integer nonlinear programming. *Energy*, *77*, 675–690.

Ko, W., & Kim, J. (2019). Generation expansion planning model for integrated energy system considering feasible operation region and generation efficiency of combined heat and power. *Energies*, *12*, 226. https://doi.org/10.3390/en12020226

Liu, C., Shahidehpour, M., Li, Z., & Fotuhi-Firuzabad, M. (2009). Component and mode models for the short-term scheduling of combined-cycle units. *Power Systems, IEEE Transactions on*, *24*, 976–990. https://doi.org/10.1109/TPWRS.2009.2016501

Lund, H., Andersen, A., Østergaard, P., Mathiesen, B., & Connolly, D. (2012). From electricity smart grids to smart energy systems – a market operation based approach and understanding. *Energy*, *42*, 96–102. https://doi.org/10.1016/j.energy.2012.04.003

Madlener, R., & Schmid, C. (2003). Combined heat and power generation in liberalised markets and a carbon-constrained world. *GAIA - Ecological Perspectives for Science and Society*, *12*, 114–120. https://doi.org/10.14512/gaia.12.2.8

Makkonen, S., & Lahdelma, R. (2006). Non-convex power plant modelling in energy optimisation. *European Journal of Operational Research*, *171*, 1113–1126. https://doi.org/10.1016/j.ejor.2005.01.020

Mitra, S., Sun, L., & Grossmann, I. E. (2013). Optimal scheduling of industrial combined heat and power plants under time-sensitive electricity prices. *Energy*, *54*, 194–211.

Morales, J. M., Conejo, A. J., Madsen, H., Pinson, P., & Zugno, M. (2014). *Integrating renewables in electricity markets* (2014th ed.). Springer. https://EconPapers.repec.org/RePEc:spr:isorms:978-1-4614-9411-9

Morales-España, G., Latorre, J., & Ramos, A. (2013). Tight and compact milp formulation of start-up and shut-down ramping in unit commitment. *IEEE Transactions on Power Systems*, *28*, 1288–1296. https://doi.org/10.1109/TPWRS.2012.2222938

Nicolosi, F., Alberizzi, J., Caligiuri, C., & Renzi, M. (2021). Unit commitment optimization of a micro-grid with a milp algorithm: Role of the emissions, bio-fuels and power generation technology. *Energy Reports*, *7*. https://doi.org/10.1016/j.egyr.2021.04.020

Ohji, A., & Haraguchi, M. (2022). 2 - steam turbine cycles and cycle design optimization: The rankine cycle, thermal power cycles, and integrated gasification-combined cycle power plants. In T. Tanuma (Ed.), *Advances in steam turbines for modern power plants (second edition)* (Second Edition, pp. 11–40). Woodhead Publishing.

Ommen, T., Brix Markussen, W., & Elmegaard, B. (2014). Comparison of linear, mixed integer and non-linear programming methods in energy system dispatch modelling. *Energy*, *74*. https://doi.org/10.1016/j.energy.2014.04.023

Bundesamt für Umwelt BAFU. (2023). *Emissionshandelsystem (EHS)*. Retrieved July 25, 2023, from https://www.bafu.admin.ch/bafu/de/home/themen/klima/fachinformationen/verminderungsmassnahmen/ehs.html

Energie Wasser Bern. (2012). Energiezentrale forsthaus - mit modernster technik bereit für morgen.

Energie Wasser Bern. (2023). *Geospeicher: Wärme für den Winter speichern*. Retrieved July 12, 2023, from https://www.ewb.ch/ueber-uns/unternehmen/kraftwerke/geospeicher.php

FICO. (2023). *FICO® Xpress Optimization*. Retrieved June 16, 2023, from https://www.fico.com/en/products/fico-xpress-optimization

Time-steps AG. (2023). *Optimization of thermal power plants*. Retrieved May 16, 2023, from https://www.time-steps.com/home.html

Saravanan, B., Das, S., Sikri, S., & Kothari, D. P. (2013). A solution to the unit commitment problem—a review. *Frontiers in Energy*, *7*(2), 223–236. https://doi.org/10.1007/s11708-013-0240-3

Seeger, T., & Verstege, J. F. (1991). Short term scheduling in cogeneration systems. *[Proceedings] Conference Papers 1991 Power Industry Computer Application Conference*, 106–112.

Singh, S. (2023). *Eu carbon price and its impact on natural gas demand*. Retrieved August 12, 2023, from https://www.gecf.org/events/expert-commentary-eu-carbon-price-and-its-impact-on-natural-gas-demand

Wang, C., Song, J., You, D., Zheng, W., Guo, J., & Zhu, L. (2022). Combined heat and power plants integrated with steam turbine renovations: Optimal dispatch for maximizing the consumption of renewable energy. *Energy Conversion and Management*, *258*, 115561.

Wang, J., You, S., Zong, Y., Træholt, C., Dong, Z. Y., & Zhou, Y. (2019). Flexibility of combined heat and power plants: A review of technologies and operation strategies. *Applied Energy*, *252*, 113445.

Zhang, Lyu, Li, Zheng, Qin, G., & Sun, Z. (2020). Research on down-regulation cost of flexible combined heat power plants participating in real-time deep down-regulation market. *Energies*, *13*, 787. https://doi.org/10.3390/en13040787

Zweifel, P., Praktiknjo, A., & Erdmann, G. (2017). *Energy economics - theory and applications*. https://doi.org/10.1007/978-3-662-53022-1

A. Linearization process of fuel consumption

The fuel consumption of CHP unit i in equation (38) must be linearized to realize MILP optimization.
In a first step, we replace the product of generation output $P_{i,t}^{CHP}/H_{i,t}^{CHP}$ and reciprocal of of the segment generation efficieny bp/bh by the function $g_{i,bp,t}^{CHP,P}$ or $g_{i,bh,t}^{CHP,H}$:

$$\begin{aligned} F_{i,t}^{CHP,P} &= \sum_{bp=1}^{N_{BP}} \left(\frac{P_{i,t}^{CHP}}{\eta_{i,bp}^{CHP,P}} * v_{i,bp,t}^{CHP,eff,P}\right) = \sum_{bp=1}^{N_{BP}} \left(g_{i,bp,t}^{CHP,P} * v_{i,bp,t}^{CHP,eff,P}\right) \quad \forall i, \forall t \\ F_{i,t}^{CHP,H} &= \sum_{bh=1}^{N_{BH}} \left(\frac{H_{i,t}^{CHP}}{\eta_{i,bh}^{CHP,H}} * v_{i,bh,t}^{CHP,eff,H}\right) = \sum_{bh=1}^{N_{BH}} \left(g_{i,bh,t}^{CHP,H} * v_{i,bh,t}^{CHP,eff,H}\right) \quad \forall i, \forall t \end{aligned} \tag{A.1}$$

In a second step, we substitute the product of variables by $\varphi_{i,bp,t}^{CHP,eff,P}$ or $\varphi_{i,bh,t}^{CHP,eff,H}$, respectively:

$$\begin{aligned} \varphi_{i,bp,t}^{CHP,eff,P} &= g_{i,bp,t}^{CHP,P} * v_{i,bp,t}^{CHP,eff,P} \quad \forall i, \forall bp, \forall t \\ \varphi_{i,bh,t}^{CHP,eff,H} &= g_{i,bh,t}^{CHP,H} * v_{i,bh,t}^{CHP,eff,H} \quad \forall i, \forall bh, \forall t \end{aligned} \tag{A.2}$$

Next, we linearize these equations based on linear inequality constraints as follows:

$$\begin{cases} \varphi_{i,bp,t}^{CHP,eff,P} \geq -v_{i,bp,t}^{CHP,eff,P} * Z \quad \forall i, \forall bp, \forall t \\ \varphi_{i,bp,t}^{CHP,eff,P} \leq v_{i,bp,t}^{CHP,eff,P} * Z \quad \forall i, \forall bp, \forall t \end{cases}$$
$$\begin{cases} \varphi_{i,bh,t}^{CHP,eff,H} \geq -v_{i,bh,t}^{CHP,eff,H} * Z \quad \forall i, \forall bh, \forall t \\ \varphi_{i,bh,t}^{CHP,eff,H} \leq v_{i,bh,t}^{CHP,eff,H} * Z \quad \forall i, \forall bp, \forall t \end{cases} \tag{A.3}$$

$$\begin{cases} \varphi_{i,bp,t}^{CHP,eff,P} \geq g_{i,bp,t}^{CHP,P} - (1 - v_{i,bp,t}^{CHP,eff,P}) * Z \quad \forall i, \forall bp, \forall t \\ \varphi_{i,bp,t}^{CHP,eff,P} \leq g_{i,bp,t}^{CHP,P} + (1 - v_{i,bp,t}^{CHP,eff,P}) * Z \quad \forall i, \forall bp, \forall t \end{cases}$$
$$\begin{cases} \varphi_{i,bh,t}^{CHP,eff,H} \geq g_{i,bh,t}^{CHP,H} - (1 - v_{i,bh,t}^{CHP,eff,H}) * Z \quad \forall i, \forall bh, \forall t \\ \varphi_{i,bh,t}^{CHP,eff,H} \leq g_{i,bh,t}^{CHP,H} + (1 - v_{i,bh,t}^{CHP,eff,H}) * Z \quad \forall i, \forall bp, \forall t \end{cases} \tag{A.4}$$

Last but not least, the fuel consumption of CHP unit i is defined as the sum of the single variables:

$$\begin{aligned} F_{i,t}^{CHP,P} &= \sum_{bp=1}^{N_{BP}} \varphi_{i,bp,t}^{CHP,eff,P} \quad \forall i, \forall bp, \forall t, \\ F_{i,t}^{CHP,H} &= \sum_{bh=1}^{N_{BH}} \varphi_{i,bh,t}^{CHP,eff,H} \quad \forall i, \forall bh, \forall t, \end{aligned} \tag{A.5}$$

where the sum of $F_{i,t}^{CHP,P}$ and $F_{i,t}^{CHP,H}$, namely $F_{i,t}^{CHP}$, describes total fuel consumption of CHP unit i at hour t. We include the latter in equation (2).

B. Logic of binary variables in TS-Energy

Combination	HHKW_Bin	HHKW_TG3_Bin	HHKW_TG2_Bin	GT_Bin	TG2_Bin	Consequences on Balance Equations
1	0	0	0	0	0	No consequence.
2	0	0	0	1	• If AHK_Heat < 26, TG2_Bin = 0 • If AHK_Heat ≥ 26 & ≤ 33.14, TG2_Bin = 0 OR 1 • If AHK_Heat > 33.14, TG2_Bin = 1	• AHK_Heat = Pre_TG2_Heat AND Pre_TG2_Heat = Heat_Extract • AHK_Heat = Pre_TG2_Heat • AHK_Heat = Pre_TG2_Heat
3	1	1	0	0	0	• HHKW_Heat = HHKW_TG3_Heat
4	1	1	0	1	• If AHK_Heat < 26, TG2_Bin = 0 • If AHK_Heat ≥ 26 & ≤ 33.14, TG2_Bin = 0 OR 1 • If AHK_Heat > 33.14, TG2_Bin = 1	• AHK_Heat = Pre_TG2_Heat AND Pre_TG2_Heat = Heat_Extract • AHK_Heat = Pre_TG2_Heat • AHK_Heat = Pre_TG2_Heat • HHKW_Heat = HHKW_TG3_Heat
5	1	0	1	0	• If HHKW_TG2 < 26, TG2_Bin = 0 • If HHKW_TG2 ≥ 26 & ≤ 31.45, TG2_Bin = 0 OR 1	• HHKW_TG2 = Pre_TG2_Heat AND Pre_TG2_Heat = Heat_Extract • HHKW_TG2 = Pre_TG2_Heat • HHKW_Heat = HHKW_TG2_Heat
6	1	0	1	1	1 (AHK_Heat_min + HHKW_TG2_min = 37.2895 > Heat_Extract_max)	• HHKW_TG2 + AHK_Heat = Pre_TG2_Heat • HHKW_Heat = HHKW_TG2_Heat

Figure B.1: Binary combinations and consequences on balance equations

C. Solution finding using branch-and-bound algorithm

As mentioned in section 3.a, MILP problems are usually solved using a linear programming based branch-and-bound algorithm. At first, FICO solver removes all integrality restrictions. The result is called the *linear-programming (LP) relaxation* of the original mixed integer programming (MIP), denoted by P_0. Next, FICO solves this *LP*. By chance, the result may satisfy all of the integrality restrictions without having them imposed explicitly. In that case, the solver stops. If not, FICO solver picks an integer variable in the LP relaxation that is fractional. For instance, the variable is x and its value in the LP relaxation is 3.7. FICO excludes this value by imposing the restrictions $x \leq 3$ and $x \geq 4$. We denote this two new MIPs by P_1 and P_2. We call the variable x the *branching variable* as we have produced two simpler sub-MIPs P_1 and P_2 with the help of x. Afterwards, FICO computes the optimal solutions for each P_1 and P_2, whereby the better solution among them will be optimal to the original problem P_0. Next, FICO applies the same procedure for P_1 and P_2. So, FICO solves the corresponding LP relaxations and if necessary, selects new branching variables. In this way, a *search tree* forms. The MIPs are called the nodes of the tree, whereas our original MIP P_0 stands for the *root node*. Figuratively, all leaves of the tree are MIPs that have not yet been branched (Benichou et al., 1971).

Suppose that our goal is to minimize costs $c^T x$ and that FICO has just solved the LP relaxation of some node in the search tree. If all integrality constraints of P_0 are satisfied in the solution at that node, we know that we have found a feasible solution. In this case, we evaluate this best integer solution by the information in section 3.a and denote it as *incumbent*. If the new feasible solution has a better objective function value than the current incumbent, then FICO records this solution as the new incumbent. Otherwise, no update is necessary. The incumbent represents a valid upper bound on the optimal solution of the given MIP. In other words, we do not accept an integer solution being higher than this value. During the branch-and-bound search, we get a valid lower bound, called the *best bound*. It is obtained by taking the minimum of the optimal objective values of all current leaf nodes. We denote the difference between the upper and best bound as *optimality gap*. Consequently, we demonstrate optimality if the gap is close to zero (Benichou et al., 1971; Dakin, 1965).

The capabilities of MIP algorithms have widely improved in recent years. The main contributors are cutting planes, heuristics, presolve, and parallelism. However, for deeper insights on these MIP methods, we refer to Benichou et al. (1971).

D. Additional figures

Profitability Analysis 2022

Month	Total Costs Actual	Total Costs Model UC2	Heat Revenue Actual	Heat Revenue Model UC2	Power Revenue Actual	Power Revenue Model UC2	Total Profit Actual	Total Profit Model UC2
Total	**EUR 31'998'064**	**EUR -1'750'079**	**EUR 9'069'536**	**EUR 9'352'078**	**EUR 73'878'366**	**EUR 46'988'741**	**EUR 50'949'838**	**EUR 58'090'898**
Jan.	EUR 9'733'402	EUR 1'450'350	EUR 1'483'530	EUR 1'590'400	EUR 11'857'873	EUR 4'515'885	EUR 3'608'001	EUR 4'655'935
Feb.	EUR 7'578'392	EUR -908'555	EUR 1'064'684	EUR 1'227'423	EUR 10'159'061	EUR 2'098'728	EUR 3'645'353	EUR 4'234'705
März	EUR 7'318'708	EUR -994'082	EUR 864'173	EUR 1'047'360	EUR 10'426'794	EUR 3'914'269	EUR 3'972'259	EUR 5'955'710
Apr.	EUR 1'335'440	EUR -559'778	EUR 795'446	EUR 821'914	EUR 4'469'731	EUR 3'447'068	EUR 3'929'737	EUR 4'828'760
Mai	EUR -1'016'056	EUR -1'026'420	EUR 546'487	EUR 449'230	EUR 2'698'110	EUR 2'782'916	EUR 4'260'653	EUR 4'258'566
Juni	EUR -1'462'883	EUR -1'484'038	EUR 348'590	EUR 323'298	EUR 2'496'980	EUR 2'675'700	EUR 4'308'454	EUR 4'483'036
Juli	EUR -920'254	EUR -1'032'030	EUR 323'869	EUR 305'717	EUR 4'877'430	EUR 5'411'502	EUR 6'121'553	EUR 6'749'250
Aug.	EUR 350'829	EUR 227'169	EUR 253'652	EUR 310'432	EUR 2'457'902	EUR 2'730'916	EUR 2'360'725	EUR 2'814'179
Sep.	EUR -922'772	EUR -871'438	EUR 478'457	EUR 458'591	EUR 3'647'902	EUR 5'411'524	EUR 5'049'131	EUR 6'741'552
Okt.	EUR -696'848	EUR -970'117	EUR 589'207	EUR 554'870	EUR 2'566'093	EUR 2'586'565	EUR 3'852'148	EUR 4'111'552
Nov.	EUR 3'756'955	EUR 49'849	EUR 976'482	EUR 905'388	EUR 7'375'652	EUR 3'954'941	EUR 4'595'179	EUR 4'810'481
Dez.	EUR 6'943'152	EUR 4'369'009	EUR 1'344'958	EUR 1'357'455	EUR 10'844'839	EUR 7'458'727	EUR 5'246'645	EUR 4'447'173

Figure D.1: Profitability analysis in 2022: actual vs. restricted model

Profitability Analysis: Model comparison

Month	Total Costs Model	Total Costs Model flexible	Heat Revenue Model	Heat Revenue Model flexible	Power Revenue Model	Power Revenue Model flexible	Total Profit Model	Total Profit Model flexible
Gesamtwerte	**EUR -1'750'079**	**EUR -1'135'917**	**EUR 9'352'078**	**EUR 9'383'549**	**EUR 46'988'741**	**EUR 48'461'517**	**EUR 58'090'898**	**EUR 58'980'982**
Jan.	EUR 1'450'350	EUR 1'279'593	EUR 1'590'400	EUR 1'589'636	EUR 4'515'885	EUR 4'384'051	EUR 4'655'935	EUR 4'694'094
Feb.	EUR -908'555	EUR -908'555	EUR 1'227'423	EUR 1'227'423	EUR 2'098'728	EUR 2'098'728	EUR 4'234'705	EUR 4'234'705
März	EUR -994'082	EUR -49'830	EUR 1'047'360	EUR 1'048'636	EUR 3'914'269	EUR 4'865'579	EUR 5'955'710	EUR 5'964'045
Apr.	EUR -559'778	EUR -607'500	EUR 821'914	EUR 824'543	EUR 3'447'068	EUR 3'459'151	EUR 4'828'760	EUR 4'891'194
Mai	EUR -1'026'420	EUR -1'064'123	EUR 449'230	EUR 459'824	EUR 2'782'916	EUR 2'889'344	EUR 4'258'566	EUR 4'413'291
Juni	EUR -1'484'038	EUR -1'501'282	EUR 323'298	EUR 327'896	EUR 2'675'700	EUR 2'711'383	EUR 4'483'036	EUR 4'540'561
Juli	EUR -1'032'030	EUR -1'040'185	EUR 305'717	EUR 307'240	EUR 5'411'502	EUR 5'422'599	EUR 6'749'250	EUR 6'770'025
Aug.	EUR 227'169	EUR 204'792	EUR 310'432	EUR 314'447	EUR 2'730'916	EUR 2'775'244	EUR 2'814'179	EUR 2'884'899
Sep.	EUR -871'438	EUR -908'057	EUR 458'591	EUR 466'739	EUR 5'411'524	EUR 5'522'895	EUR 6'741'552	EUR 6'897'691
Okt.	EUR -970'117	EUR -962'448	EUR 554'870	EUR 566'171	EUR 2'586'565	EUR 2'856'770	EUR 4'111'552	EUR 4'385'389
Nov.	EUR 49'849	EUR 337'236	EUR 905'388	EUR 905'382	EUR 3'954'941	EUR 4'263'843	EUR 4'810'481	EUR 4'831'989
Dez.	EUR 4'369'009	EUR 4'084'442	EUR 1'357'455	EUR 1'345'613	EUR 7'458'727	EUR 7'211'929	EUR 4'447'173	EUR 4'473'100

Figure D.2: Profitability analysis in 2022: restricted vs. flexible model

Consumption Analysis 2022

Month	Wood Actual	Wood Model UC2	Waste Actual	Waste Model UC2	Total Gas Actual	Total Gas Model UC2
Gesamtwerte	**MWh 255'083**	**MWh 296'350**	**MWh 481'729**	**MWh 557'757**	**MWh 335'238**	**MWh 65'826**
Jan.	MWh 25'059	MWh 27'138	MWh 42'136	MWh 51'294	MWh 94'850	MWh 22'175
Feb.	MWh 22'817	MWh 24'864	MWh 39'321	MWh 46'330	MWh 78'345	MWh 0
März	MWh 24'888	MWh 27'200	MWh 37'299	MWh 51'294	MWh 54'880	MWh 0
Apr.	MWh 21'386	MWh 25'168	MWh 43'880	MWh 49'640	MWh 16'222	MWh 3'112
Mai	MWh 22'901	MWh 26'524	MWh 48'145	MWh 51'294	MWh 115	MWh 0
Juni	MWh 6'056	MWh 10'485	MWh 45'021	MWh 49'640	MWh 0	MWh 0
Juli	MWh 19'248	MWh 24'882	MWh 43'064	MWh 51'294	MWh 4	MWh 0
Aug.	MWh 23'049	MWh 27'515	MWh 15'341	MWh 18'201	MWh 538	MWh 0
Sep.	MWh 16'844	MWh 25'556	MWh 43'656	MWh 48'054	MWh 256	MWh 0
Okt.	MWh 24'350	MWh 24'637	MWh 44'627	MWh 51'294	MWh 1'597	MWh 1'074
Nov.	MWh 23'192	MWh 26'377	MWh 42'844	MWh 49'640	MWh 43'879	MWh 10'185
Dez.	MWh 25'292	MWh 26'004	MWh 36'396	MWh 39'781	MWh 44'553	MWh 29'281

Figure D.3: Consumption analysis in 2022: actual vs. model

Consumption Analysis 2022

Month	Wood flexible Model	Waste flexible Model	Total Gas flexible Model
Gesamtwerte	**MWh 291'012**	**MWh 557'739**	**MWh 72'366**
Jan.	MWh 27'138	MWh 51'294	MWh 20'901
Feb.	MWh 24'864	MWh 46'330	MWh 0
März	MWh 27'125	MWh 51'294	MWh 4'992
Apr.	MWh 24'847	MWh 49'640	MWh 2'862
Mai	MWh 25'407	MWh 51'294	MWh 0
Juni	MWh 9'976	MWh 49'640	MWh 0
Juli	MWh 24'629	MWh 51'294	MWh 0
Aug.	MWh 26'807	MWh 18'201	MWh 0
Sep.	MWh 24'393	MWh 48'054	MWh 0
Okt.	MWh 23'479	MWh 51'294	MWh 2'006
Nov.	MWh 26'377	MWh 49'640	MWh 13'864
Dez.	MWh 25'969	MWh 39'762	MWh 27'740

Figure D.4: Consumption analysis in 2022: flexible model

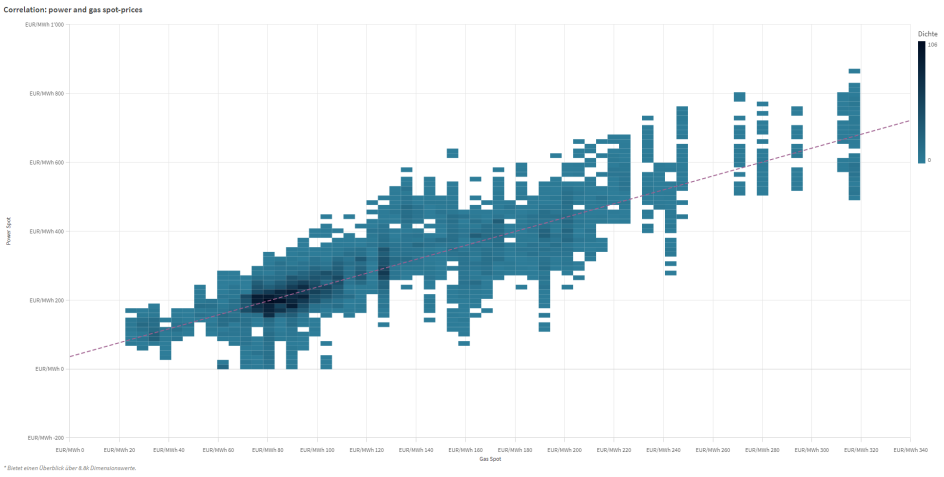

Figure D.5: Correlation in 2022: power and gas spot prices in EUR/MWh

Declaration of consent

on the basis of Article 30 of the RSL Phil.-nat. 18

Name/First Name: Schmidt Annika

Registration Number: 17-318-122

Study program: MSc in Climate Sciences

Bachelor ☐ Master ☑ Dissertation ☐

Title of the thesis: Optimal Operation and Analysis of the ”Energiezentrale Forsthaus”: A Unit Commitment Approach using Mixed Integer Linear Programming

Supervisor: Prof. Dr. Doina Radulescu

I declare herewith that this thesis is my own work and that I have not used any sources other than those stated. I have indicated the adoption of quotations as well as thoughts taken from other authors as such in the thesis. I am aware that the Senate pursuant to Article 36 paragraph 1 litera r of the University Act of 5 September, 1996 is authorized to revoke the title awarded on the basis of this thesis.

For the purposes of evaluation and verification of compliance with the declaration of originality and the regulations governing plagiarism, I hereby grant the University of Bern the right to process my personal data and to perform the acts of use this requires, in particular, to reproduce the written thesis and to store it permanently in a database, and to use said database, or to make said database available, to enable comparison with future theses submitted by others.

Bern, 25.08.2023

Place/Date

A. Schmidt

Signature